AD-A064 395 AIR FORCE INST OF TECH WRIGHT-PATTERSON AFB OHIO SCH--ETC F/G 20/5
GYROSCOPE ERROR MODEL INVESTIGATION FOR THE SPERRY SLIC-15 RING--ETC(U)
DEC 78 P A RENAUD

UNCLASSIFIED AFIT/GA/EE/78-5 NL

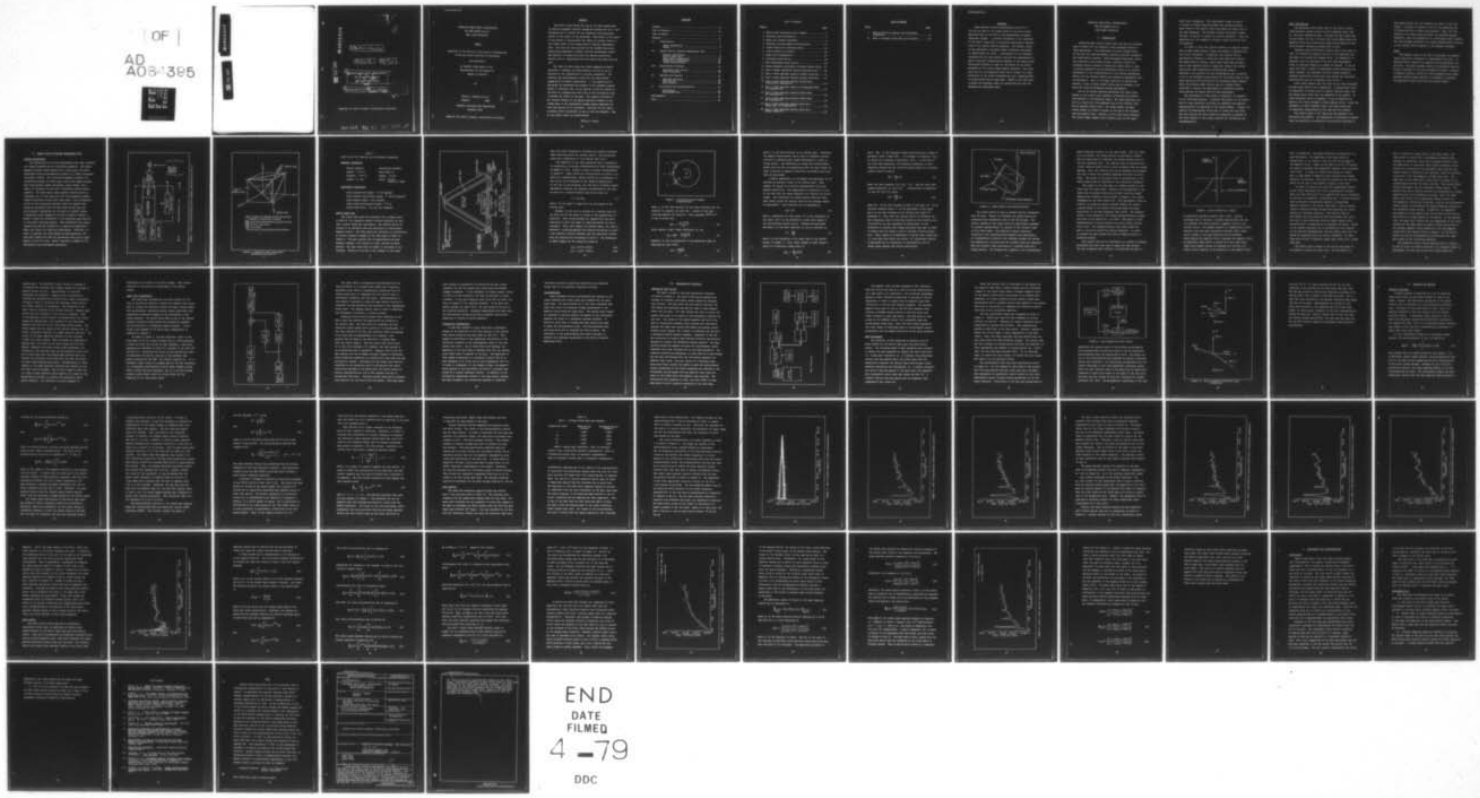

END
DATE FILMED
4-79
DDC

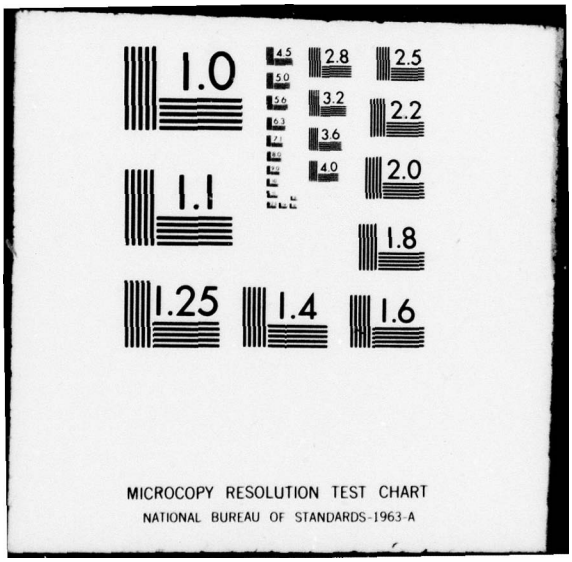
1.0
1.1
1.25
1.4
1.6
1.8
2.0
2.2
2.5
2.8
3.2
3.6
4.0
4.5
5.0
5.6
MICROCOPY RESOLUTION TEST CHART
NATIONAL BUREAU OF STANDARDS-1963-A

LEVEL II

(1)

AD A064395

DDC FILE COPY

(9) Master's thesis

(11) Dec 78 (12) 73 p.

(6) GYROSCOPE ERROR MODEL INVESTIGATION FOR THE SPERRY SLIC-15 RING LASER GYROSCOPE.

THESIS

(14) AFIT/GA/EE/78-5

(10) Philip A. Renaud
~~Captain~~ USAF

DDC RECEIVED FEB 12 1979 A

Approved for public release; distribution unlimited.

012 225 79 01 30 100

AFIT/GA/EE/78-5

GYROSCOPE ERROR MODEL INVESTIGATION FOR THE SPERRY SLIC-15 RING LASER GYROSCOPE

THESIS

Presented to the Faculty of the School of Engineering
of the Air Force Institute of Technology

Air University

in Partial Fulfillment of the
Requirements for the Degree of
Master of Science

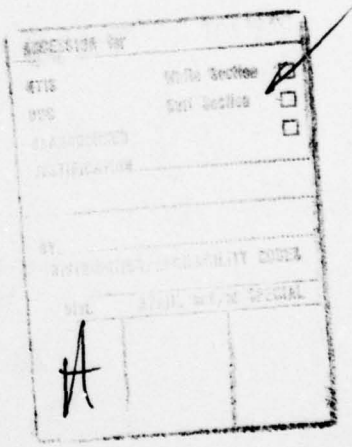

by

Philip A. Renaud B.S.A.E.
Captain USAF

Graduate Astronautical Engineering
December 1978

Approved for public release, distribution unlimited.

Preface

The recent trend toward the use of the laser gyroscopes in various strapdown inertial navigation systems has led to the increased need to define the low frequency noise producing drifts in the output of the gyroscope. This study is the result of my attempt to characterize the effect of optical dither on the output noise of the Sperry SLIC-15 Inertial Measurement Unit. The test unit was received by the AFIT/EN Electrical Engineering Department in March 1978 and considerable effort was required to design and build the various electronics modules used to communicate with and record test data from the unit.

The idea for this report was first suggested by Major Salvatore R. Balsamo, my thesis advisor as well as my instructor in the complexities of inertial navigation. His patience and understanding, along with his many helpful suggestions is greatly appreciated. I also gratefully acknowledge the assistance and support of my classmate Captain Robert S. Lawrence, who, in the pursuit of his own thesis on the SLIC-15, designed and built much of the electronics used to access the output of the gyro. The support furnished by Mr. Kenneth Thomson of the Sperry Gyroscope Company in providing many of the unpublished company papers regarding the test unit proved to be invaluable. And last but not least, a sincere debt of gratitude is due my wife and daughter. May we once again renew our acquaintances.

Philip A. Renaud

Contents

Preface ii

List of Figures iv

List of Tables v

Abstract vi

I. Introduction 1

Basic Assumptions 3
Scope 4

II. Sperry SLIC-15 Inertial Measurement Unit 5

General Description 5
SLG-15 Laser Gyro 8
Laser Gyro Compensation 20
Temperature Compensation 23
Q-flex Accelerometer 24

III. Experimental Procedure 25

Laboratory Test Set-up 25
Test Procedures 27

IV. Analysis and Results 32

Analysis Technique 32
Test Results 37
Error Models 47

V. Conclusions and Recommendations 59

Conclusions 59
Recommendations 60

Bibliography 62

Vita 63

List of Figures

Figure		Page
1	SLIC-15 IMU Functional Block Diagram	6
2	Sensitive Axes Orientation	7
3	Laser Gyro Optical Schematic	9
4	Rotating Circular Sagnac Interferometer	11
5	Output Mirror and Combining Prism	14
6	Lock-in Effects on Output	16
7	Laser Gyro Compensation	21
8	Laboratory Test Set-up	26
9	Gyro Operational Mode Control	29
10	Sensor Assembly Orientation Utilized During Tests	30
11	Gyro C Normal Operation Output Autocorrelation	40
12	Gyro C Power Spectral Density--Normal Operation	41
13	Gyro C Power Spectral Density--Normal Operation	42
14	Gyro C Power Spectral Density--Fixed Bias, Alternating Compensation	44
15	Gyro C Power Spectral Density--Alternating Bias, No Compensation	45
16	Gyro C Power Spectral Density--Fixed Bias, No Compensation	46
17	Gyro A Power Spectral Density--Fixed Bias, No Compensation	48
18	Gyro C Power Spectral Density Curve Fit-- Fixed Bias, No Compensation	53
19	Gyro C Power Spectral Density Curve Fit-- Normal Operation	56

List of Tables

Table		Page
I	SLIC-15 S/N 002 Physical and Performance Parameters.	8
II	Gyro C--Average Output Mean and Variance.	38

Abstract

Power spectral density measurements from 10^{-3} to 8.33 Hz are made of the output noise of the SLG-15 laser gyroscope used in the SLIC-15 IMU manufactured by Sperry Gyroscope Company. A detailed discussion of the operation of the SLG-15 laser gyro is presented along with a description of its optical dither mechanism. The digital output of the gyroscope is analyzed using correlation techniques to characterize the noise. A description of the analysis technique and the test station used for the measurements is given along with representative samples of the output noise. Particular attention is paid to the effect of the dither mechanism on the output power density spectrum. The tests show that the low frequency noise due to dither is a characteristic of the dither mechanism and not a characteristic of a particular SLG-15 laser gyro. Based on the test data a linear low frequency model is constructed for both the dithered and undithered case.

GYROSCOPE ERROR MODEL INVESTIGATION FOR THE SPERRY SLIC-15 RING LASER GYROSCOPE

I. Introduction

During the past several years there has been an increased need to define the low frequency noise producing drifts in laser gyroscopes. This requirement has been brought about by the need for high performance precision inertial navigation and stabilization systems. Data processing algorithms, generally referred to as Kalman filters, provide a method for combining various sources of system and sensor data in order to produce navigation system performance which is an optimal combination of the characteristics of the various subsystems. Errors from the various sensors are modeled by appropriate random processes. Thus, if the gyro noise can be defined and modeled, a more accurate Kalman filter may be designed to enhance the inertial navigation system performance.

One of the unique problems associated with laser gyroscopes is the output noise created by dithering the optical bias applied to the gyroscope input. The laser gyroscope output is a function of the algebraic sum of the rotation input and an applied optical bias. For large inputs, the gyro output signal is linearly related to the sum of the rotation rate and applied bias. However, as the input sum is reduced, the output signal departs from linearity and, as the input

nears zero, disappears. This phenomenon, known as lock-in is caused by energy coupling between the counter-rotating laser beams in the optical cavity and makes the beams lock to the same frequency. The minimum rotation input which causes the gyro to unlock, is called the lock-in threshold. Thus, the gyroscope will not respond to rotation inputs below the lock-in threshold.

In order to avoid the lock-in problem, the applied optical bias is made large enough to force the system to operate above the lock-in threshold. In addition, the optical bias is periodically reversed to remove any long term drift effects. The Sperry SLIC-15 system, unlike other laser gyro systems, uses a Kerr magnetic mirror to apply and reverse the optical bias rather than mechanically dithering the mirrors. Therefore, the objective of this investigation was to develop a set of low frequency error models for the Sperry SLIC-15 ring laser gyroscope with and without the dithering signal applied. These error models might then be used in a Kalman filter algorithm to improve the performance of navigation systems incorporating the Sperry SLIC-15 laser gyroscopes.

The development of this study is presented, by chapters, in the following sequence. A general description of the Sperry SLIC-15 laser gyroscope including its operation and physical characteristics is presented in the second chapter. Chapter III details the experimental setup used to record the test data. The test results and error models are presented in Chapter IV. The final chapter of this study contains the conclusions and recommendations.

Basic Assumptions

The gyroscope error models were in the form of linear time-invariant systems driven by white Gaussian noise; that is, they were shaping filters. Although the gyro system may be non-linear, the use of linear error state space models and shaping filters has yielded good results when applied to previous inertial navigation systems (Ref 1:3-26).

Gaussian noise distribution implies that at any point in time, the probability density function of the amplitude has the shape of a normal bell shaped curve. The assumption of Gaussian noise is justified by the fact that measurement noise is typically caused by a number of sources. It can be shown that when a number of independent random variables are added together, the resultant function closely matches a Gaussian probability distribution even though the individual distributions may not be Gaussian (Ref 2:8-21).

White noise implies that the noise is not time correlated and has equal power at all frequencies. Although white noise is impossible in nature since it implies infinite power, one can assume white noise over the bandwidth of the system. If time-correlated noise is required, it can be generated by passing white noise through a linear shaping filter. Under the assumption of white Gaussian noise, the noise vector may be completely characterized by the mean and the variance.

The random output of the laser gyro was assumed to be stationary and ergodic. The assumption of stationarity implies that the statistics or probability distribution functions of

the random process are not affected by a shift in the time origin. A process is ergodic if all of its statistics can be determined from a single time function. Thus, the time average of an ergodic process equals the ensemble average. Therefore, under the assumption of a stationary erodic process, the time averages performed on a single representative function of the ensemble may be equated to the ensemble averages.

Scope

The digital output of the SLIC-15 gyroscope is analyzed using correlation techniques to characterize the noise. An autocorrelation function is computed from the gyroscope output data. The power spectral density is determined from the Fourier transform of the autocorrelation function. Finally, a transfer function, driven by a white Gaussian noise power spectral density input function, is designed to reproduce the gyroscope output noise with and without dither.

II. Sperry SLIC-15 Inertial Measurement Unit

General Description

The Sperry SLIC-15 Inertial Measurement Unit (IMU) consists of a sensor assembly and an electronics assembly. The sensor assembly contains three Sperry SLG-15 laser gyros and three Sundstrand Q-flex accelerometers mounted on a common orthogonal structural element. The electronics assembly contains the electronics modules for laser gyro control and signal processing, accelerometer signal processing, power supply, and a module to interface the IMU with a navigation system digital computer. The laser gyros sense angular rotation about an orthogonal set of body axes while the accelerometers measure linear acceleration along their input axes. This information is fed to the electronics assembly where the applied bias rates are subtracted from the gyro data and the gyro and accelerometer information are converted to digital format. A functional block diagram of the IMU is shown in Figure 1. Figure 2 shows the orientation of the sensitive axes relative to the sensor mounting surface. This orientation was chosen because this IMU was intended to be used in an application where very high roll rates were anticipated. Therefore, in order to equalize the rates sensed by each gyroscope, the axes were canted such that all gyroscopes would see an equal amount of the roll rate. Table I presents a summary of the IMU physical and performance parameters.

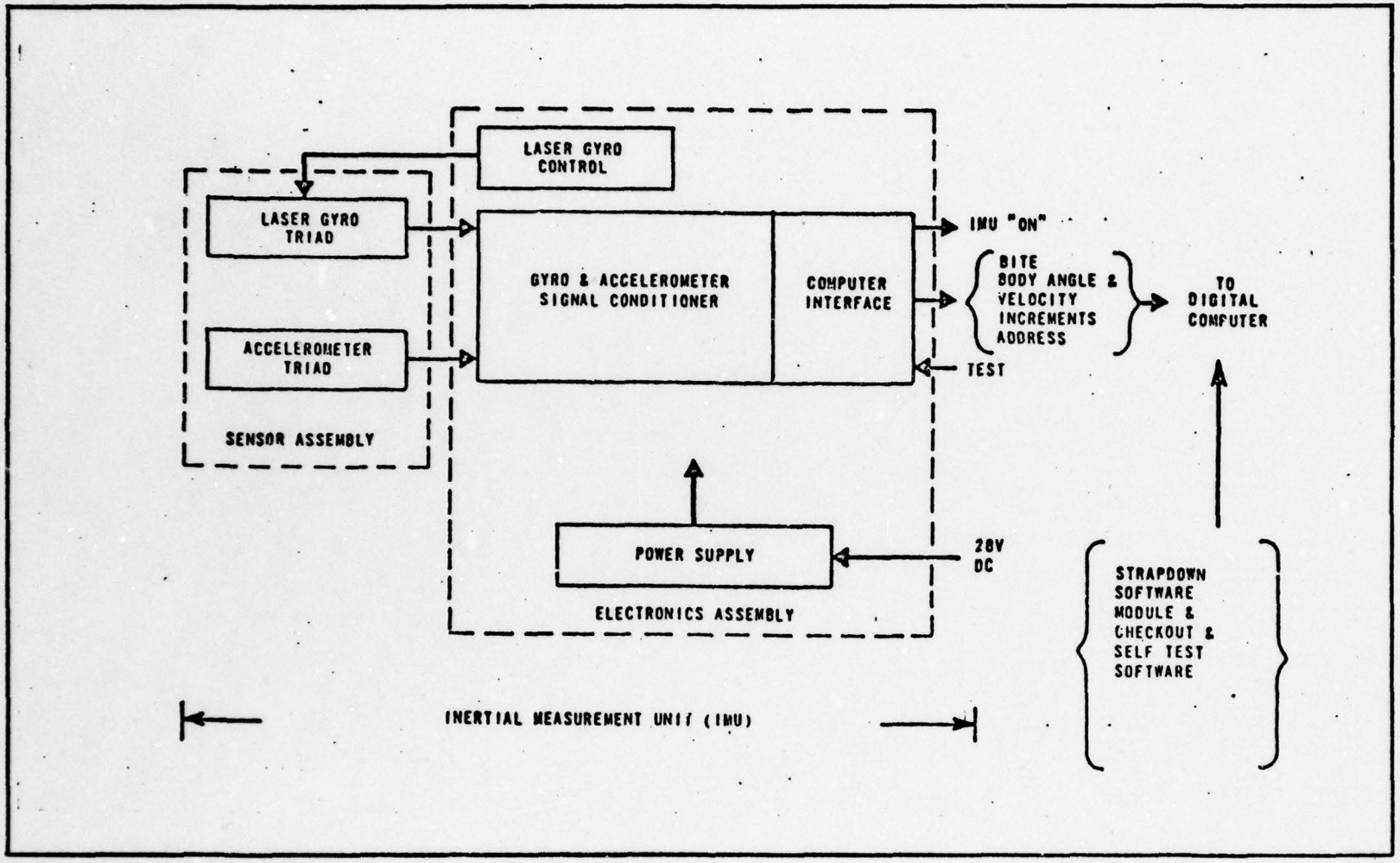

Figure 1 SLIC-15 IMU Functional Block Diagram (Extracted from Ref 3)

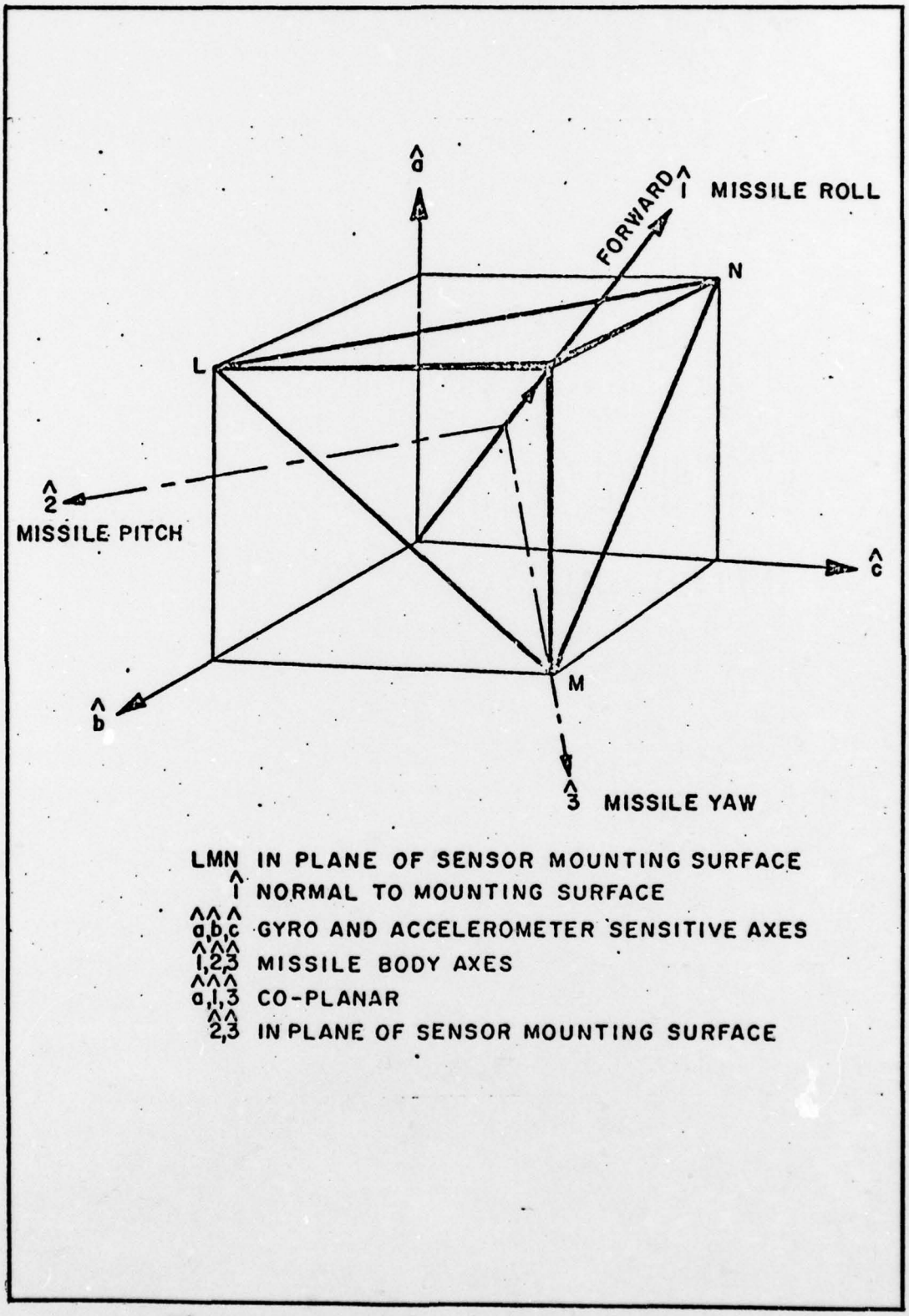

Figure 2 Sensitive Axes Orientation
(Extracted from Ref 3)

Table I

SLIC-15 S/N 002 Physical and Performance Parameters

Physical Parameters

Sensor Assembly	Electronics Assembly
Length: 8.50 in.	Size 8x9x7 in.
Diameter: 7.38 in.	Weight: 16 lbs.
Weight: 23 lbs.	Power: 28 VDC fused at 6 amps

Performance Parameters

Input Angular Rate Range: ± 650 deg/sec.

Input Angular Acceleration Range: ± 60,000 deg/sec^2

Input Angular Range: Full Freedom

Input Linear Acceleration Range: ± 10 g

Output Resolution: 13.3 arc sec (nominal)

SLG-15 Laser Gyro

The three laser gyros are machined into a single block of CER-VIT (low expansion ceramic vitreous material) so that their optical paths are intertwined. The optical cavity is mounted in an evacuated case and protected by a multi-layer magnetic shield. The three gyros are identical in construction. An optical schematic diagram of the laser gyro is shown in Figure 3. The gyro optical path is approximately an equilateral triangle, 4.87 inches on a side, defined by three mirrors. The gyro input axis is normal to the plane of the triangle. Mounted in one leg of the triangle is the laser

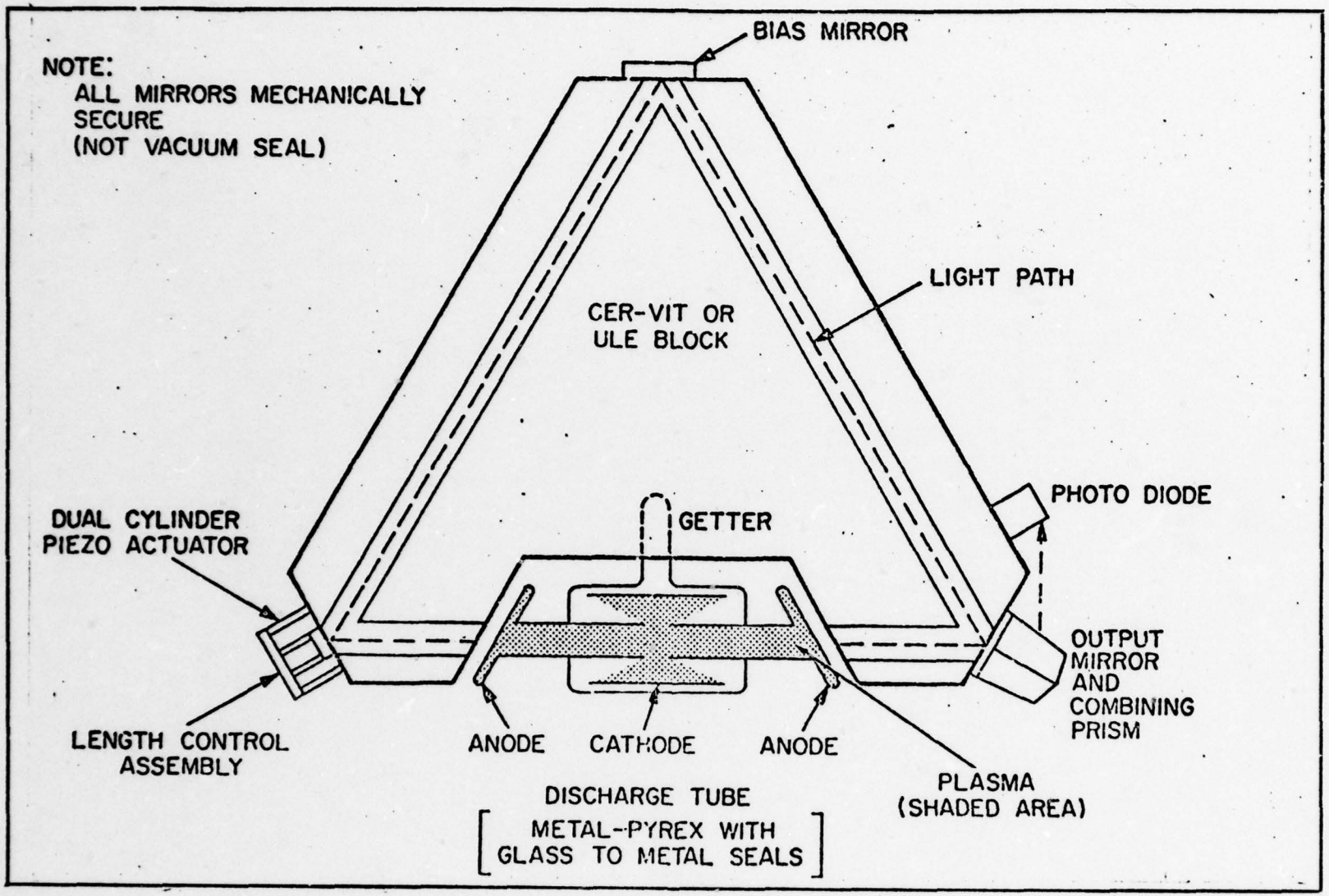

Figure 3 Laser Gyro Optical Schematic (Extracted from Ref 3)

gain tube which generates a clockwise and counter-clockwise beam traveling around the optical cavity. The helium-neon laser has a wavelength of 1.15 microns (Ref 3:14).

The operation of the laser gyroscope may be understood by considering a rotating interferometer as first demonstrated by Sagnac in 1913. Figure 4 shows a circular interferometer of radius R. Light enters the interferometer at point A, is split by a beamsplitter, travels around the circumference of the circle, and recombines at the original beamsplitter. If the unit is non-rotating, the time for a clockwise traveling beam to complete one complete circumference is the same as that for a counterclockwise beam and is given by

$$t = 2\pi R/c \tag{1}$$

where c is the speed of light and R is the radius of the optical path.

However, if the unit is rotated at a constant speed Ω, the time for the two beams to return to the beamsplitter is different. This occurs because the beamsplitter has moved from point A while the light is traveling around the interferometer. Thus, with respect to inertial space, the beam or wavefront, traveling against the rotation recombines at point B and travels a shorter distance than the beam which travels with the rotation and recombines at point C. The difference in path lengths for the respective beams is

$$ct_+ = 2\pi R + R\Omega t_+ \tag{2a}$$

$$ct_- = 2\pi R - R\Omega t_- \tag{2b}$$

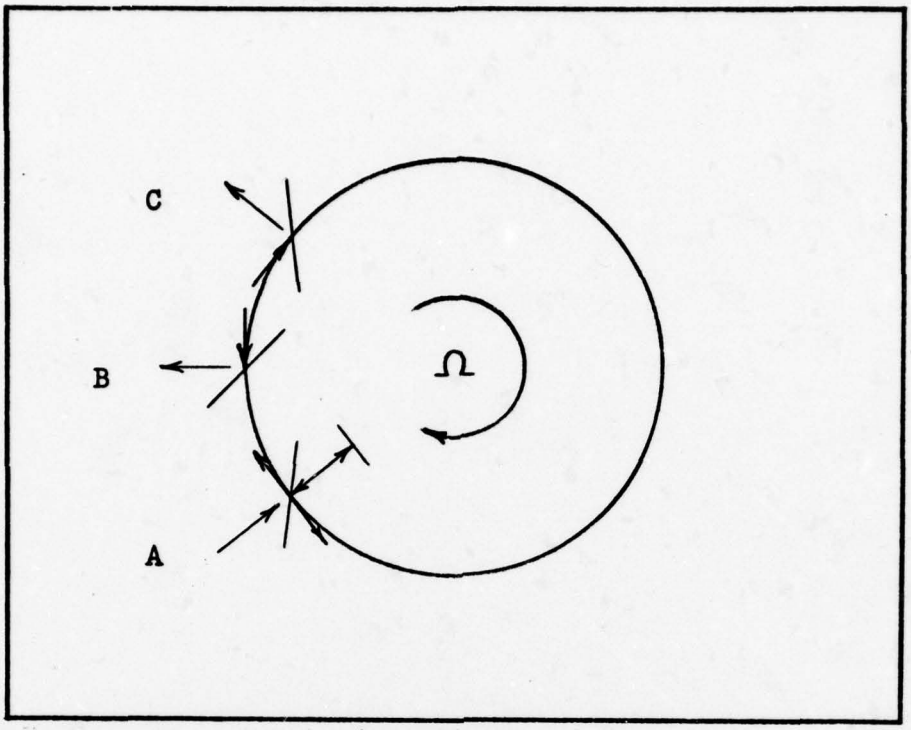

Figure 4 Rotating Circular Sagnac Interferometer

where t_+ is the time required for the beam traveling with the rotation to complete one path and t_- refers to the beam traveling against the rotation. Thus, assuming $R^2\Omega^2 << c^2$ it can be shown that

$$\Delta t = \frac{4\pi R^2 \Omega}{c^2} \tag{3}$$

which implies a path length difference ΔL as

$$\Delta L = c\Delta t = \frac{4\pi R^2 \Omega}{c} \tag{4}$$

Equation (4) can be generalized to any geometric shape by rewriting as (Ref 4:481)

$$\Delta L = \frac{4A\Omega}{c} \tag{5}$$

where A is the area enclosed by the optical path. Therefore, the Sagnac interferometer can be used to determine inertial rotation by measuring path length differences in terms of fringe shifts. The difficulty in using this interferometer arises from its lack of sensitivity since the path length for light traveling in opposite directions is normally much less than one wavelength.

A marked improvement on the Sagnac interferometer can be realized by placing a laser in the optical path. This changes the system to an active interferometer with much greater sensitivity. The improvement in sensitivity is due to the fact that the laser frequency is a function of cavity length. The conditions for lasing require that the total path length around the optical cavity be an integral number of wavelengths. This condition can be expressed as

$$n\lambda = P \tag{6}$$

where n represents the mode number, λ is the wavelength of the laser, and P is the perimeter or total path length of the non-rotating optical cavity. Knowing the wavelength and speed c of the wave, Equation (6) can be rewritten as

$$f = \frac{nc}{P} \tag{7}$$

where f is the frequency of the laser beam in the optical cavity of length, P. Thus, small changes in path length P result in a frequency change given by

$$\Delta f_{\pm} = \frac{nc}{P^2} \Delta P_{\mp} \tag{8}$$

where $\Delta f_{\pm}$ is the frequency change resulting from a change in perimeter (path) length $\Delta P_{\mp}$. An increase in frequency (Δf_+) is caused by a decrease in perimeter (ΔP_-). In the case of the ring laser gyroscope, the frequency difference or beat frequency between the two counter-rotating beams in a rotating optical cavity is merely

$$\Delta f = \frac{nc}{P^2} \Delta L \tag{9}$$

where the beat frequency $\Delta f = \Delta f_+ - \Delta f_-$ and the total path length difference $\Delta L = \Delta P_- - \Delta P_+$. Substitution of Equations (5) and (6) into (9) yields

$$\Delta f = \frac{4A}{\lambda P} \Omega \tag{10}$$

where Δf is the beat frequency output of the gyro, Ω is the inertial rotation input, λ is the wavelength of the laser, and A is the area enclosed by the optical path length of perimeter P. Thus, when the optical cavity is rotating, the beat frequency output is directly related to the rotation rate. In actuality the beat frequency is proportional to any difference in optical path length and great care must be taken to insure that the output is due to inertial rotation inputs only. Other causes of a difference in optical path length are; (1) a net gas flow within the cavity, (2) anisotropic effects of materials due to differences in polarization, and (3) unique phase changes upon mirror reflections.

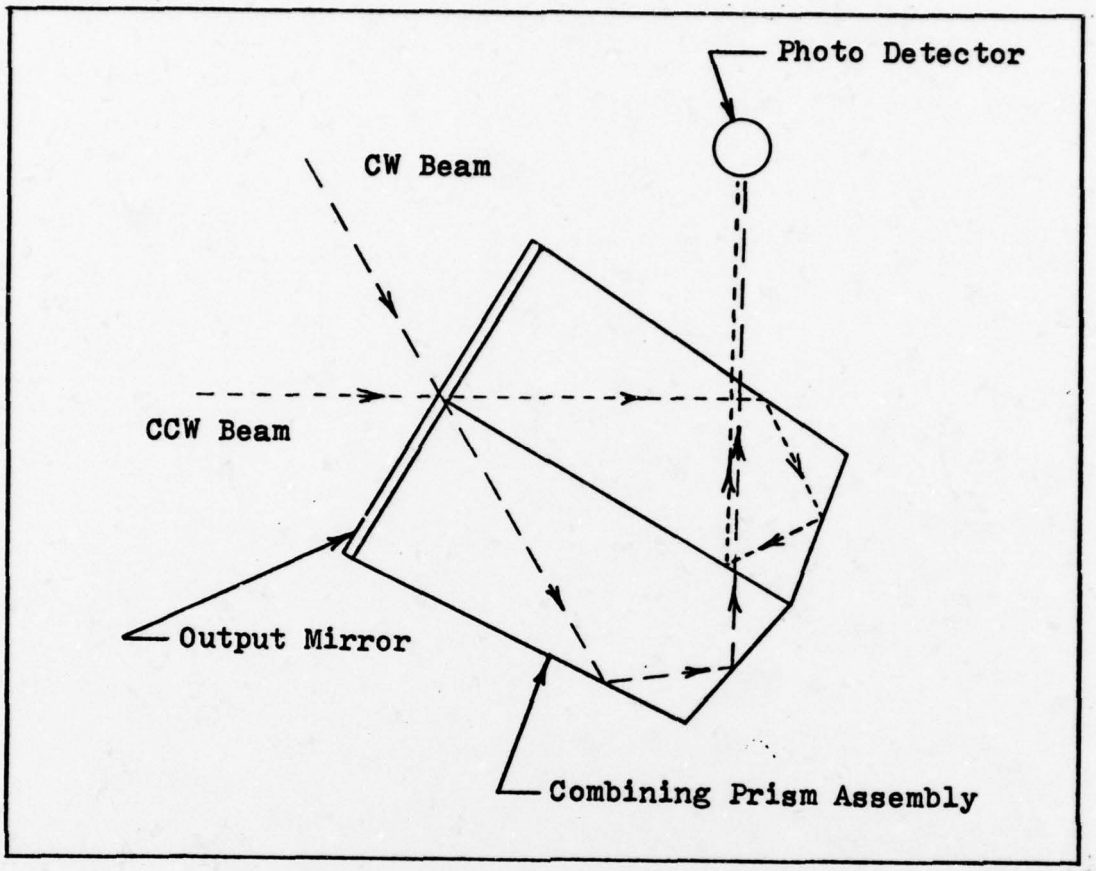

Figure 5 Output Mirror and Combining Prism

The output mirror is used to extract optical information from the gyro. Figure 5 illustrates the output mirror and combining prism combination used on the SLG-15 gyro. The optical coating of the output mirror is specifically designed to transmit approximately 0.1 percent of the incident light of both laser beams. The beams are totally internally reflected by the combining prism assembly and superimposed on a beamsplitter located at the interface between the prisms. The beamsplitter reflects half the incident light and transmits half the incident light resulting in a combined beam and a fringe pattern. The fringes are a measure of the instantaneous

phase difference between the two laser beams. When the laser is not rotating, the fringe pattern is stationary, however, when the laser gyro is rotating, the fringe pattern moves at the beat frequency rate. The combined beam is projected onto a photo detector whose field of view is smaller than the fringe spacing. Thus, the rotation rate can be measured by recording the rate at which the intensity maximums move past the photo diode. The output of the photo diode is proportional to the input rotation and is digitized in the electronics assembly.

The output of the laser gyro is linearly related to the input rate for large rates. However, as the magnitude of the input rate is reduced below some critical value the signal departs from linearity, and as shown in Figure 6, the output disappears as the input nears zero. This phenomenon, known as lock-in, is caused by energy coupling between the counter-rotating beams in the optical cavity and makes the beams synchronize to the same frequency (Ref 5:148). The dominant source of the coupling is the mutual backscattering of energy from each of the beams into each other. The source of this backscattering is the multilayer dielectric mirror coating (Ref 5:153). The minimum rotation input that causes the gyro to unlock is called the lock-in threshold. In order to operate the gyro outside the lock-in region the gyro is optically biased.

The optical bias can be introduced by a number of methods. Techniques that have been used to apply the bias include the use of magneto-optic effects, or subjecting the gyro to

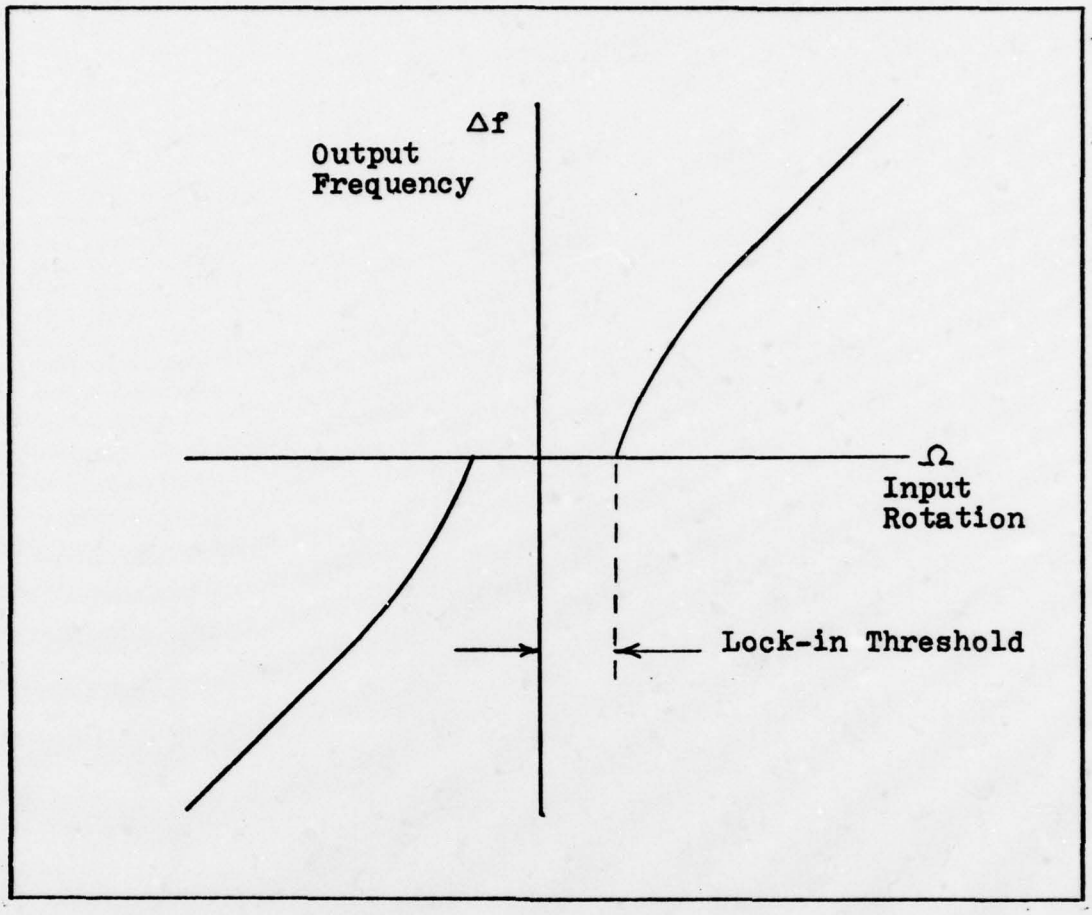

Figure 6 Lock-in Effects on Output

an additional physical rotation (Ref 5:156). Another technique used to provide a constant bias involves the use of a Faraday cell which produces a magnetic field in the optical cavity. The Faraday element is a magnetically active material such that when circularly polarized light, whose vector rotates in the same direction as the windings which produce the magnetic field, traverses the magnetic field an additional phase shift is picked up by the light beam. Light which passes through the Faraday cell and has a rotation vector opposite to the direction of the magnetic field

will be unaffected. The phase difference is equivalent to a path difference. The magnitude of the phase shift is proportional to the length of the cell and the strength of the magnetic field. Biases on the order of 10^5 to 10^6 deg/hr are easily obtainable with reasonable magnetic field strengths (Ref 5:158). In order to utilize this system in a laser gyro, a high degree of magnetic field stability and thermal stability is required. The stability problem is the limiting factor in the use of this system to apply a fixed bias.

In order to overcome the stability requirement inherent in any fixed bias system the bias is periodically reversed. Thus, any long term drift of the applied bias may be eliminated by the use of a symmetric, alternating bias. A method currently used by Honeywell Incorporated applies an alternating physical rotation to the entire laser gyro. This is accomplished by spring mounting the gyro and operating the entire system as a torsional pendulum. Bias rates as high as 2000 deg/hr have been achieved with this system (Ref 5:162). The bias is then subtracted from the output signal either electronically or mechanically to determine the input. Errors in the biasing technique can be minimized with the symmetry of the bias and increasing the time per dither cycle that the system is operating above the lock-in threshold. An ideal bias would utilize a symmetric square wave dither with a large bias rate.

The system used by Sperry on the SLG-15 laser gyro is an attempt to achieve an ideal bias. The bias mirror is

used to introduce a phase shift in the laser beams. The bias mirror is coated with a ferromagnetic material that changes its refractive index with an applied electric field. The phase shift or equivalent path length difference occurs because two components of the polarized laser beam see different indices of refraction and therefore travel at different velocities in the ferromagnetic coating (Ref 6:59). The magnitude of this phase shift varies with the square of the voltage applied across the mirror coating. This system offers several advantages over the mechanical dither system. The applied bias can be rapidly reversed by alternating the voltage applied across the ferromagnetic coating. Thus, the ideal square wave dither can be approached without concern for the mechanical limitations (vibration, inertia, and acceleration loads) imposed by alternating the applied physical rotation in the mechanical dither system. In addition, the magnitude and symmetry of this applied bias can be easily controlled by monitoring the voltage applied to the mirror. On the negative side, the phase shift varies with the temperature of the mirror coating and the bias cannot be readily turned off because of the residual magnetic field remaining in the ferromagnetic coating when the electric field is removed. In the SLIC-15 system the bias is electronically extracted from the laser gyro output in the electronics assembly.

The perimeter control mirror assembly shown in Figure 3 is used to servo the savity perimeter to an integral number of wavelengths for which the helium neon lasing medium has

maximum gain. The perimeter control mirror is mounted on a piezoelectric actuator that changes length as a voltage is applied across the unit. Approximately 70 volts per wavelength are required. Length control is achieved by exciting the piezoelectric actuator with a small alternating voltage in order to oscillate the perimeter control mirror by a small fraction of wavelength. The intensity of the laser beam is monitored by an optical detector. Maximum gain occurs when the intensity of the beam is a maximum. Thus, if the perimeter control mirror is dithered about the cavity length for maximum gain, the intensity of the beam drops whenever the mirror is not at the proper cavity length. The dither signal and the output of the optical detector are, in effect, multiplied together in a phase sensitive detector. The output of the phase sensitive detector is then filtered to give a dc error signal. When the system is operating at maximum gain, the value of the error signal will be zero. However, whenever the cavity length needs adjustment, the intensity of the beam will fall as the perimeter control mirror is moved away from the maximum gain position and, conversely the intensity of the beam will rise when the mirror is moved toward maximum gain point. Multiplication of these signals in the phase sensitive detector will produce an output with a net dc average. The dc error signal is then fed to a high voltage amplifier which applies a dc signal to the piezoelectric actuator to position the perimeter control mirror properly. The direction of mirror movement is

determined by the sense of the error signal. This insures operation of the gyro at the peak gain of the lasing medium.

Laser Gyro Compensation

The laser gyro compensation circuitry located in the SLIC-15 electronics assembly contains the digital logic necessary to convert the optically biased ring laser output signal into synchronized, accurately scaled, serial pulse data that represents incremental changes in the orientation of the sensor assembly. The serial pulse data is fed to the digital computer interface module within the electronics assembly for multiplexing to a navigation system computer. A functional block diagram of the SLG-15 gyro compensation is presented in Figure 7.

As shown in Figure 7, the raw sinusoidal output of the ring laser is fed to a pulse forming circuit, which generates a pulse for every four cycles of beat frequency. Each pulse represents an increment of about 13.3 seconds of arc (Ref 3:26 and Ref 7:4). Resolution as low as 3.3 arc seconds per pulse is attainable but was not used due to the rotation rate regime intended for the IMU. The circuit consists of: (1) a comparator whose output is a square wave at the beat frequency, (2) a monostable multivibrator circuit which outputs a pulse train at twice the beat frequency, and (3) a two bit up-down counter circuit whose output is a pulse train 1/8 the frequency of the input pulse train.

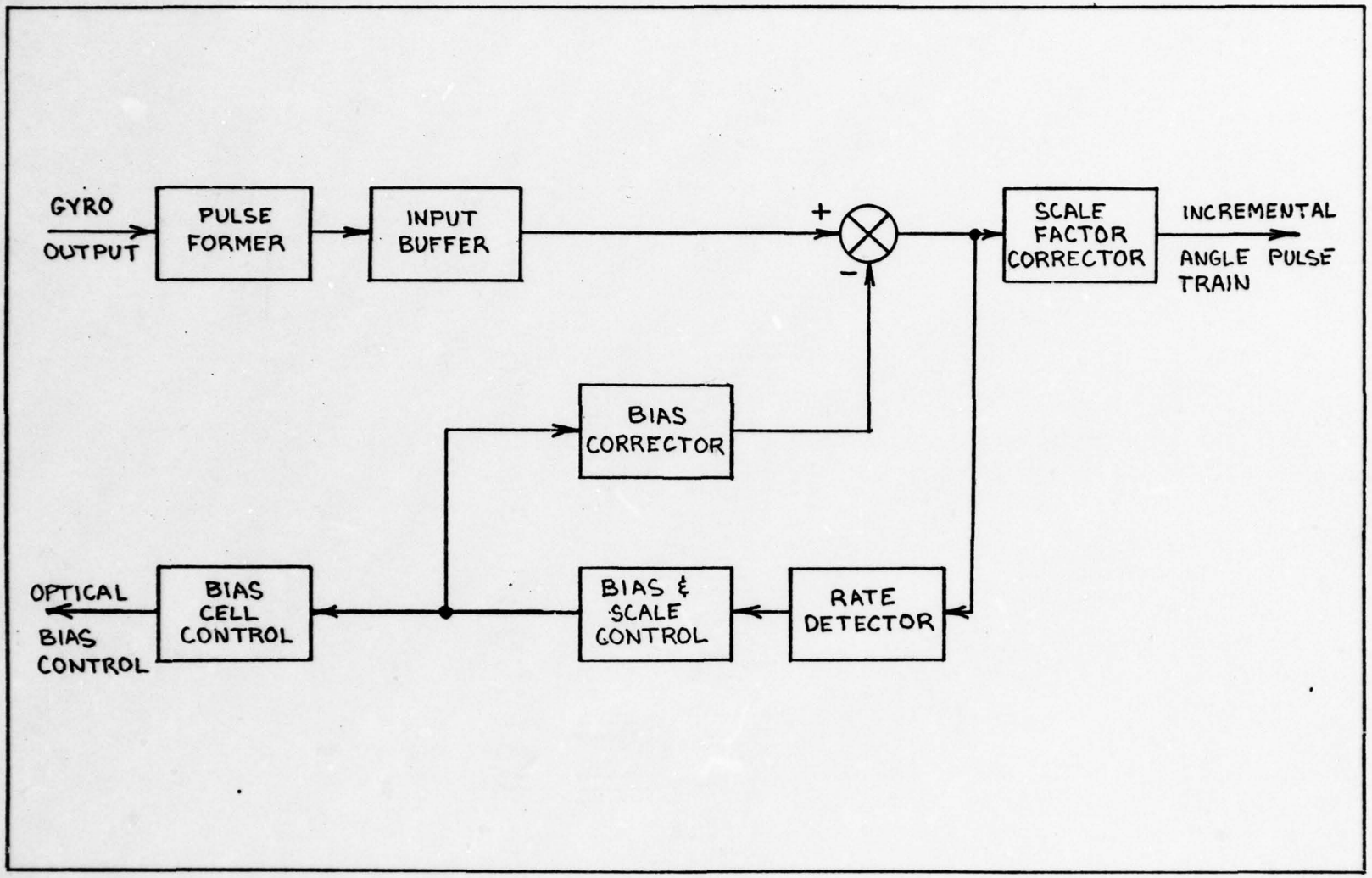

Figure 7 Laser Gyro Compensation

The pulse train is subsequently synchronized with the bias excitation in a clocked input buffer and a digitally generated pulse train is algebraically subtracted from the output pulse train to compensate for the optical bias intentionally imposed on the ring laser. Synchronization of the signals is assured by using the same control circuits to establish the bias excitation and polarity of the compensating pulse train. The imposed optical bias is fixed in magnitude but alternates in polarity 1.5 times a second.

Normally a rate detector senses input rotations to the SLG-15 gyro and controls the application and polarity of the optical bias. The rate detector integrates the bias corrected output pulses over a period of 10 milliseconds. If the count reaches 78 in this time interval, which corresponds to an input rate of approximately 29.0 deg/sec., the applied bias is fixed in the direction to operate away from the lock-in region. When the pulse count falls below 74 in this time interval (27.3 deg/sec) the bias returns to the alternating mode of operation. However, SLIC-15 S/N 002 was modified for use by Hughes Aircraft Company in laboratory tests simulating operation on a missile with very high rate and acceleration inputs. Utilization of the normal rate detector operating on the relatively slow 10 millisecond time cycle, would allow the gyro to be driven into the lock-in region by angular accelerations as low as 1800 deg/sec over the 10 millisecond time cycle. Therefore Sperry developed an atypical rate detector for the SLIC-15 S/N 002 system. This high speed

bias tracker is implemented by monitoring the gyro output frequency via the raw square wave coming from the Schmidt trigger comparator. If the frequency is between preset limits, (25 kHz to 70 kHz nominally) the bias is switched 1.5 times a second. If the gyro frequency goes below the low limit, the bias is toggled to the opposite polarity. If the gyro frequency exceeds the upper limit, the bias polarity is held in the existing direction. Frequency measurements are made every 331 microseconds thereby providing an angular acceleration capability in excess of 60,000 deg/sec^2.

Temperature Compensation

It has been observed in gyro tests that a systematic change in the magnitude of the bias produced by the optical bias mirror occurs as the gyro heats up (Ref 9:3). This change is attributed to the temperature sensitivity of the dielectric constant of the ferromagnetic layer of the bias mirror (Ref 6:69). Due to bias mirror self heating, the magnitude of the bias shows a decrease with time for several hours after power is applied to the gyro. The magnitude of this change corresponds to a decrease of about 1600 Hz in beat frequency on a 5 hour run at room temperature (Ref 8:5). In order to compensate for the change in bias, the magnetic field applied to the bias mirror is held at a constant magnitude by a current regulator circuit. In addition to correcting for temperature effects of the bias mirror, heaters are used throughout the electronics assembly to stabilize

individual precision operational amplifiers and reference diodes used in the precision regulator circuits.

Accelerometers

Three Sundstand Q-flex accelerometers are mounted in the sensor assembly with their input axes aligned with the gyro input axes. The accelerometer is of the force rebalance type where the output is an analog voltage proportional to the specific force along the input axis. The analog output signal is converted to precise digital increments in the electronics assembly for input to a navigation systems computer. It should be noted that no attempt was made during this study to model the accelerometer noise. The accelerometers were only used as an aid in aligning the SLIC-15 gyros. The discussion of the accelerometers was merely included to complete the technical description of the SLIC-15 Inertial Measurement Unit.

III. Experimental Procedure

Laboratory Test Set-up

The basic concept of the data acquisition technique is shown in Figure 8. The SLIC-15 IMU sensor assembly was mounted on a Genisco rate-table using a specially designed test fixture. The rate table was only used to position the IMU during the experiment and was not used to input angular rates into the gyro. The test fixture was built to allow the sensor input axes to be placed in any orientation required for the test. The output of the sensor assembly was fed to the SLIC-15 electronics assembly which contains the electronics modules for laser gyro control and signal processing, sensor assembly power supply, and a module to interface the IMU with a navigation system digital computer. Operation of the IMU was controlled by using a data monitor/controller specifically designed to replace the navigation system computer. The data monitor/controller samples the gyro and accelerometer output registers over time intervals set by the pulse generator. The register contents are displayed, in octal form on an LED display and are also multiplexed from the electronics assembly via parallel data lines. The six, twelve bit (including sign), data words which contain the number of gyro and accelerometer pulses accumulated in the output registers are buffered in the multiplexer and processed into six parallel data lines for input to the Cipher Model 85H magnetic tape recorder. The multiplexer also attaches an octal code word (4444) to each data group to aid in machine processing of the test data.

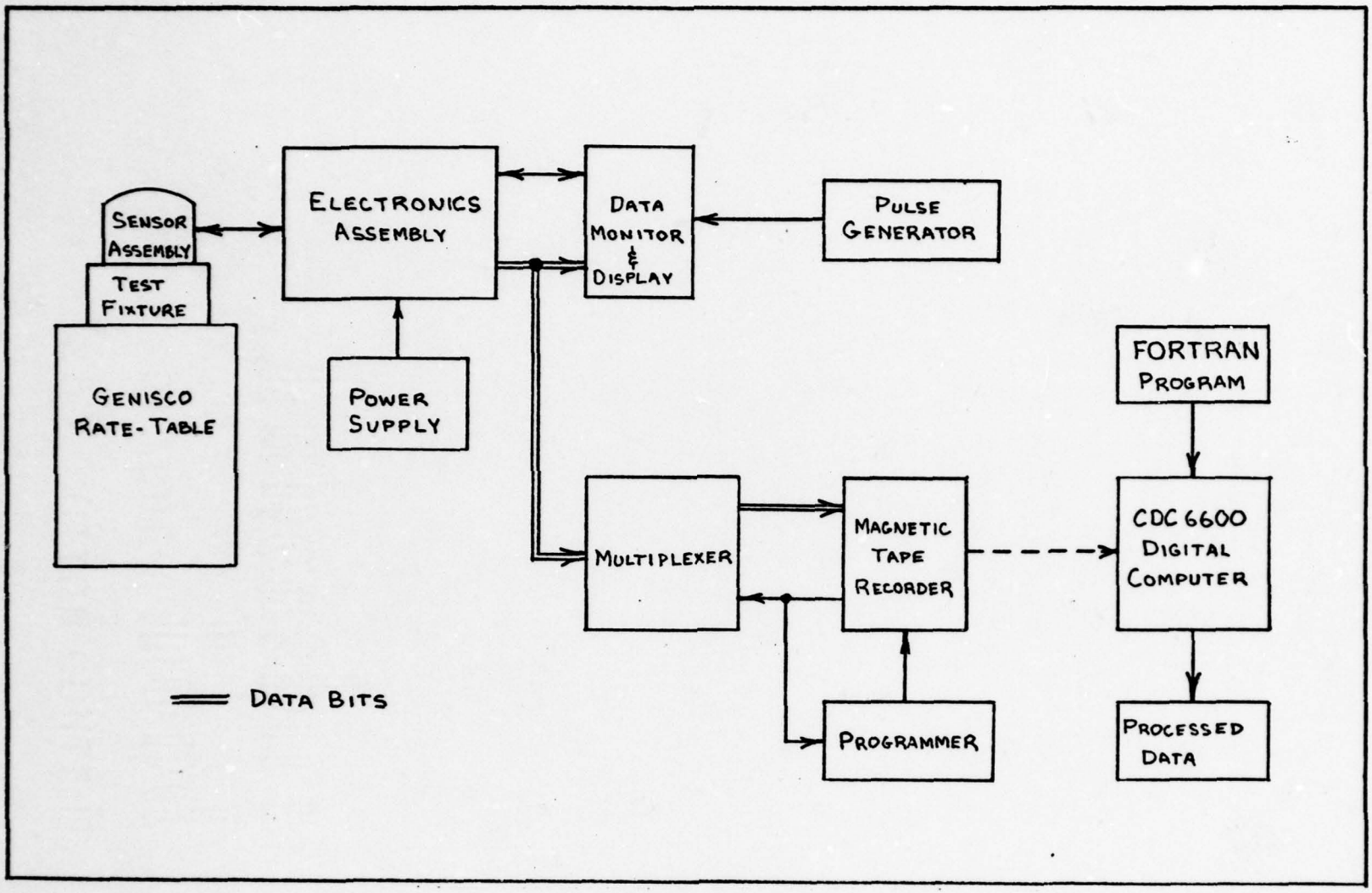

Figure 8 Laboratory Test Set-up

The magnetic tape recorder operates in the continuous mode and records the data at a rate of 20,000 characters/sec. at a tape speed of 25 inches/sec. The electronic programmer applies a short interrecord gap every 10 seconds or 200,000 characters in order to comply with the magnetic tape read limitations of the CDC 6600 digital computer. The recorded magnetic data tape is read by the CDC 6600 computer which utilizes a FORTRAN search routine to find the octal code (4444) attached to each data group. The data group is then sorted by the FORTRAN routine into incremental gyro and accelerometer pulse data. Thus, the data output represents the total number of individual gyro or accelerometer pulses accumulated over the sample period set in the pulse generator.

Test Procedures

The objective of this study was to develop a set of error models for the SLG-15 laser gyro with and without dither. The following modes of gyro operation were utilized to gather the data necessary to support the test objectives: (1) normal gyro operation, (2) a constant, non-alternating optical bias was applied while the pulse train which algebraically subtracts the optical bias from the gyro output remained operational and alternating, (3) a normal, alternating optical bias was applied to the gyro while the algebraic bias compensation pulse train was turned off and, (4) a constant optical bias was applied and the algebraic bias compensation was turned off.

Since the optical bias is introduced to the system via the magnetic bias mirror, simply turning off the electronic command to the mirror would leave a residual magnetic field in the mirror coating which would decay at an unknown rate. Therefore, all tests conducted without optical dither were accomplished with a constant optical bias applied to the system. Each gyro is controlled by a separate but identical electronics card in the electronics assembly.

The four operational modes were commanded as shown in Figure 9. Normal gyro operation was commanded by closing switches one and two. Removing the dither completely was accomplished by opening both switches. This automatically applied a fixed bias to the bias mirror. However, opening of switch two did not apply a fixed compensation to the gyro output. Thus, the large resultant bias was removed from the gyro data within the data reduction program. The optical bias was held constant by closing switch one while the algebraic or bias compensation was removed by closing switch two. Therefore, the test data was collected with: (1) all switches open, (2) switch one only closed, (3) switch two only closed, and finally (4) all switches closed.

The accelerometer input axes were positioned as shown in Figure 10. For the purpose of this study it was assumed that the accelerometer and gyro input axes were coaligned. This assumption is essentially correct except for the small misalignment angles incurred during manufacture of the IMU sensor assembly. Orientation of the axes was accomplished by

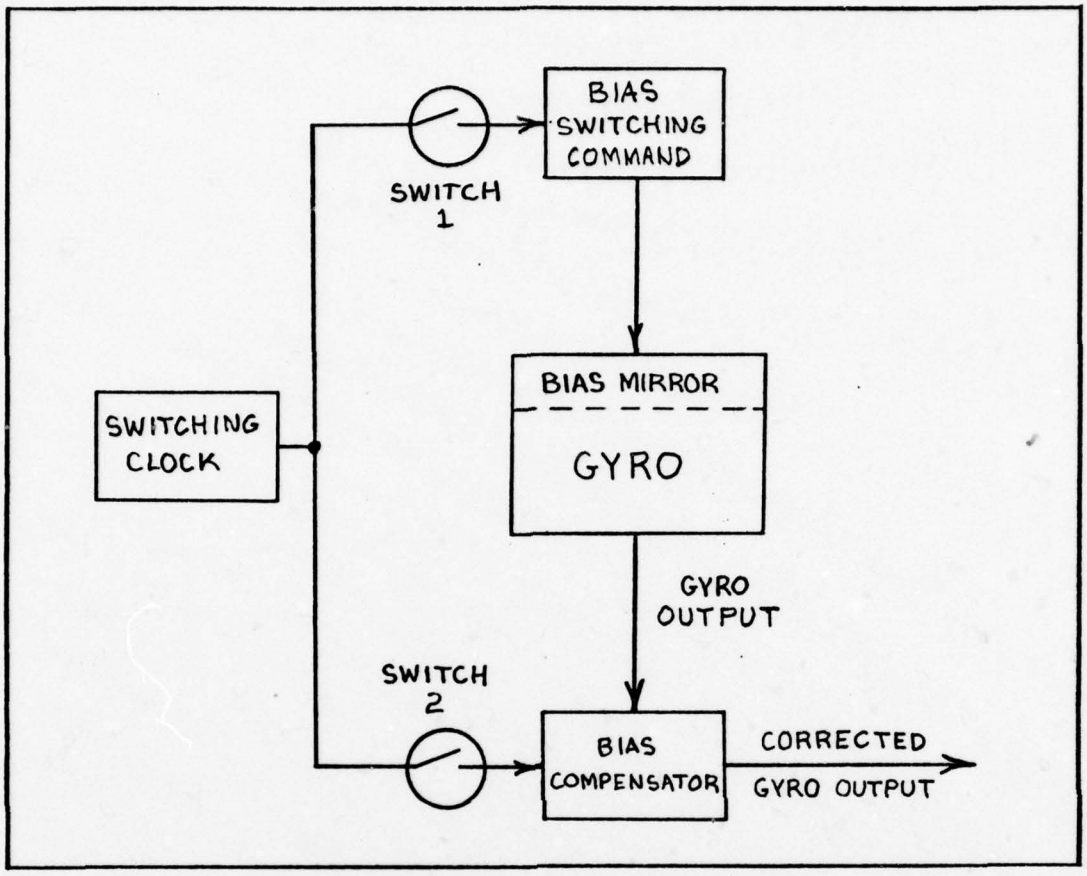

Figure 9 Gyro Operational Mode Control

maximizing the analog output of the vertical accelerometer and simultaneously nulling the output of the two horizontal accelerometers while the system was at rest. The analog output of the accelerometers was displayed on digital voltmeters during this operation. All testing was accomplished with the system stationary in the local geographic coordinate system. Thus, the only inertial input to the gyros was the particular component of earth rate sensed by the gyros at the test site. The test site was located at Room 238, Building 640, Wright-Patterson AFB, Ohio. The geographical coordinates of the test

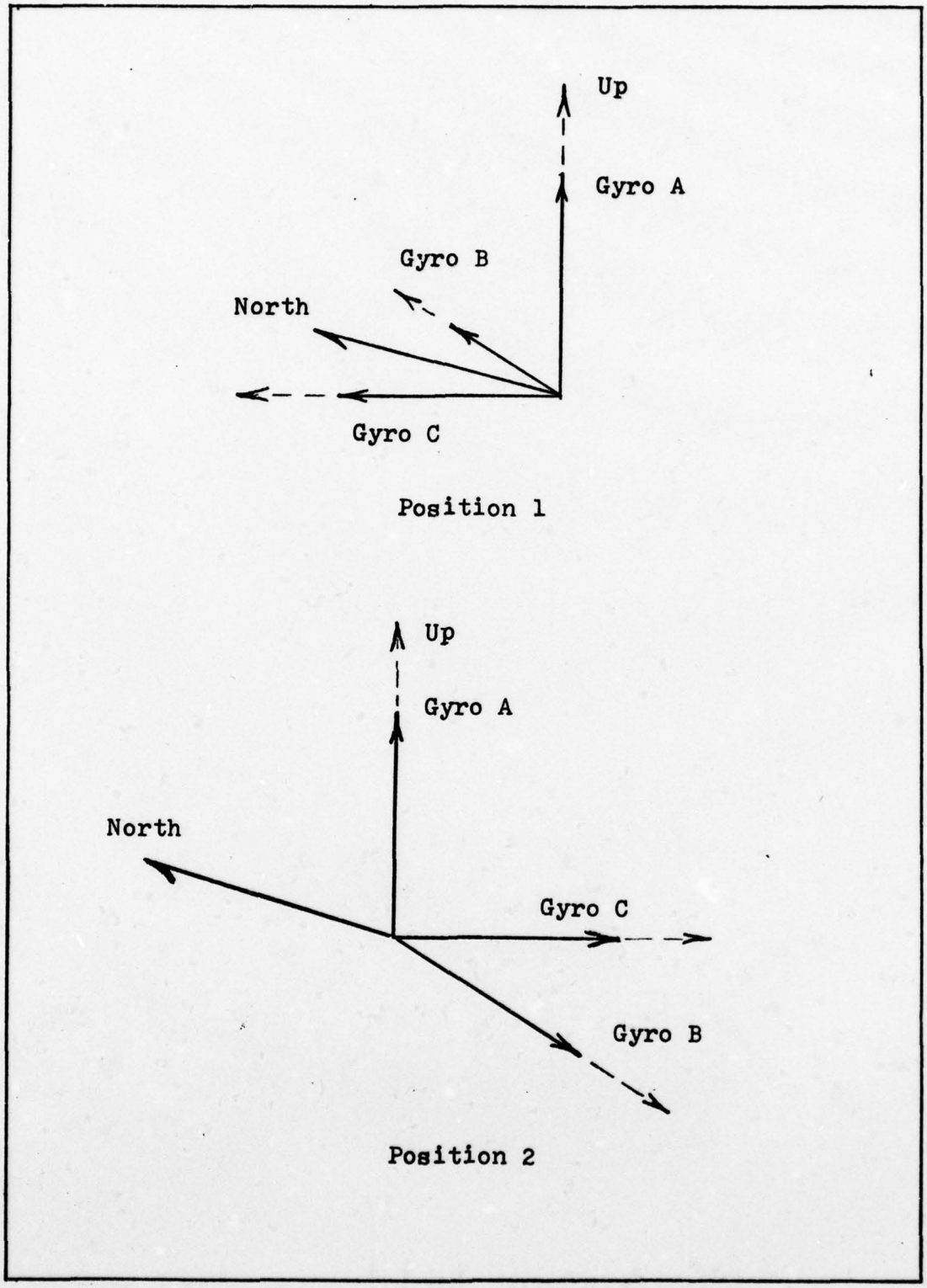

Figure 10 Sensor Assembly Orientation Used During Test

site are 39° 47' 17" North latitude and 84° 05' 45" West longitude at an elevation of 830 feet above mean sea level. The IMU was allowed to warm-up and stabilize a minimum of 30 minutes after turn on before collecting test data. Due to tape reel size limitations, the maximum continuous data sample time was 510 seconds. Approximately ten seconds of test words were recorded at the beginning and end of each data sample to verify proper operation of the test instrumentation during the data run. After a "quick look" at the test data for obvious system malfunctions, the test data was read into the CDC 6600 digital computer for subsequent data reduction and analysis.

IV. Analysis and Results

Analysis Technique

A random process is described by a set of functions whose exact values at any future instant in time are unknown. However, the statistical properties of the random function can be described by a joint probability distribution. Therefore, at any given point in time, there is a definite probability that the function will lie between specified values. A stationary random process is one in which its associated probability distribution functions do not change with time. Thus, for a stationary random function, each sample of the function is statistically equivalent to every other equal time sample.

If $f_1(t)$ represents a member of a stationary random process, the autocorrelation of $f_1(t)$ is defined as

$$\phi_{11}(\tau) = \lim_{T\to\infty} \frac{1}{T} \int_0^{\tau} f_1(t) f_1(t+\tau)\, dt \qquad (11)$$

This assumes that the random process is also ergodic. For a stationary ergodic random process, the autocorrelation function is the same for each sample period and a characteristic of the entire random process. Through the use of an autocorrelation function, the power spectral density of the random process and be found. The relationship between the autocorrelation function and the power spectral density function

is given in the Weiner-Khitchine theorem as

$$\Phi_{11}(\omega) = \int_{-\infty}^{\infty} \phi_{11}(\tau)\, e^{-j\omega\tau}\, d\tau \tag{12}$$

and

$$\phi_{11}(\tau) = \frac{1}{2\pi} \int_{-\infty}^{\infty} \Phi_{11}(\omega)\, e^{j\omega\tau}\, d\omega \tag{13}$$

Thus, the autocorrelation function and power spectral density function are Fourier transform pairs. The value of the autocorrelation function is a maximum at $\tau = 0$ and is

$$\phi_{11}(0) = \lim_{T\to\infty} \frac{1}{T} \int_{0}^{\infty} f_1^2(t)\, dt \tag{14}$$

which is the square of the standard deviation or the variance (for zero mean). It should also be noted that if the random function contains a hidden periodic component, then the autocorrelation function will also contain components of the same frequency, although any phase information that the periodic component may have had is lost. Similarly, the power spectral density function computes power density spectra rather than the amplitude or phase spectra of the random signal.

The output noise distribution of the SLG-15 laser gyro was assumed to match a Gaussian probability distribution. Therefore, under this assumption, the only major pieces of information required to model the random output of the gyro were the mean, the variance, and the power spectral density

or autocorrelation function of the output. In order to complete the analysis, it was also necessary to demonstrate repeatability of the output signal by comparing data from different equal time samples. The test data was sampled every 0.01 seconds. Thus, according to the "sampling theorem" of Shannon, the highest useful Fourier component was $1/2 \Delta T$ or 50 Hz. However, to obtain a power spectral density estimate with a frequency resolution f, data must be taken over a period of 1/f seconds. Thus for gyro noise power spectral densities to 10^{-3} Hz, data must be taken for 1000 seconds. The Cipher Model 85H magnetic tape recorder reel size limitations along with the tape speed required for proper byte density limited the recorded data period to approximately 480 seconds. Thus, the maximum frequency resolution attainable during this analysis was 0.002 Hz. However, during the course of the experiment, it was determined that the upper cutoff frequency of interest would be in the 8 to 10 Hz range which required that the data be sampled every 0.05 to 0.0625 seconds. Therefore, the raw test data was read from the magnetic tape into the CDC 6600 computer where a total of six 0.01 second sample periods were integrated to create each computer data point. This yielded an upper cutoff frequency of 1/.12 or 8.33 Hz.

The autocorrelation function of the sample was computed using the International Math and Statistics Library (IMSL) subroutine FTAUTO. This routine computes the mean, $\bar{x}$,

and the variance, σ^2, using

$$\bar{X} = \frac{1}{N} \sum_{i=1}^{N} X_i \tag{15}$$

and

$$\sigma^2 = \frac{1}{N} \sum_{i=1}^{N} (X_i - \bar{X})^2 \tag{16}$$

where x_i is the individual data point and N is the total number of data points. The autocorrelation function was computed from

$$\phi_j = \frac{\frac{1}{N} \sum_{i=1}^{N-j} (x_i - \bar{x})(x_{i+j} - \bar{x})}{\sigma^2} \qquad j = 0, 1, \cdots, N-1 \tag{17}$$

The power spectral density was determined from the Fourier transform of the autocorrelation function. This was accomplished using the IMSL FTFFT1 subroutine which utilizes a fast Fourier transform algorithm.

A problem of leakage is inherent in the Fourier analysis of any finite record of data (Ref 10:46). The record has been formed by looking at the actual signal for a period of N seconds and by neglecting everything that happened before or after this period. The Fourier transform of a continuous cosine will be represented by an impulse at a frequency f. However, if a finite sample is chosen, this is equivalent to multiplication by a data window in the time domain which is in turn equivalent to performing a convolution in the frequency domain. Thus, if the impulse function at f is

convolved with the Fourier transform of the square data window, the result will be a function with an amplitude of the form (sin x)/x centered about f.

This function is no longer localized on the frequency axis but has a series of sidelobes. Therefore, in order to localize the contribution of a given frequency by reducing the sidelobes a small spectral window which has lower sidelobes in the frequency domain than the larger rectangular data window is applied to the time series. Therefore, the routine first calculated a symmetric spectral window

$$W_j = 1 - \left| \frac{j - \left(\frac{L-1}{2}\right)}{\frac{L+1}{2}} \right| \quad j = 0, 1, \cdots, L-1 \qquad (18)$$

where L is a power of 2 used to segment the time series. In order to reduce the contribution of the sidelobes, the IMSL routine suggests that the data be divided into a minimum of 16 segments. The fast Fourier transform of each segment was then computed using

$$\Phi_{k+1} = \sum_{j=0}^{L-1} \phi_{j+1} e^{2\pi i j k/N} \qquad (19)$$

where k = 0, 1, ..., L-1. The spectral estimates were made for each segment of length L. The estimates for the N/L segments were then averaged and scaled on output from the FTFFT1 subroutine. The output of the two subroutines, which represented the autocorrelation function and power spectral density was then plotted using an Air Force Institute of

Technology subroutine, DRAWZ, which self-scales the data to maximize the data spread on the plot.

Several important points regarding the analysis scheme are worth noting. The output of the autocorrelation routine has the mean removed. In order to calculate the true mean and variance of a periodic signal, the data must be analyzed over complete cycles. This was necessary because a time average instead of ensemble average was used to estimate the mean and variance. This was particularly important when analyzing data collected during test runs where neither the alternating optical bias nor the algebraic compensation pulse train were operational at the same time. In these modes of operation, the gyro output would have a square wave, at the dither frequency, superimposed on the output. Therefore, the data was analyzed for 172 dither cycles or 229.28 seconds. This allowed two completely independent data runs to be recorded on one 480 second data tape. The absolute frequency resolution attainable for the data run was 1/229.28 or .004 Hz.

Test Results

The means and variances computed during the various Gyro C test runs are shown in Table II. The variances were computed with the square wave removed from the test data. The means were corrected for any component of earth rate imposed on the gyro by averaging the means between data runs with the gyro input axes oriented 180° apart. This was justified by the fact that the difference between the means for identical input axis

Table II

Gyro C - Average Output Mean and Variance

Operational Mode*	Mean/.06 sec (Pulses)	Variances/.06 sec (Pulses^2)
I	-.1594	.3904
II	-.4216	.3532
III	-.5587	.4159
IV	-.6291	.3699

*Mode I--Normal gyro operation; Mode II--Constant optical bias, alternating algebraic compensation; Mode III Alternating optical bias, no algebraic compensation; Mode IV--Constant optical bias, no algebraic compensation.

orientations typically was on the order of 0.67 arcseconds/sec. or less while the differences between data runs with the input axis oriented 180^o apart were 6.67 arcseconds/sec. or greater. Thus, the turn-on to turn-on variation was at least an order of magnitude smaller than the variation due to earth rate. The magnitude of the earth rate component sensed by the gyro is consistent with the test orientation of the gyro input axes. The exact alignment of the North and East vectors in the inertial laboratory was not measured for this experiment. This is due to the fact that the rate table was used to orient the Gyro C axis 180 degrees apart in the local horizontal plane between data runs. The output of the accelerometers was used to insure that the system remained in the horizontal

plane after being repositioned. The readout accuracy of the accelerometers was 1 milli-g allowing the table to remain level to within 3 minutes of arc. Thus with the exception of the turn-on to turn-on variation, the difference in output means for the two orientations was twice the component of earth rate sensed by the gyro.

The output autocorrelation for normal operation of Gyro C is shown in Figure 11. The graph was typical of the autocorrelation plots obtained during the experiment. The low frequency oscillation of the autocorrelation function occurs at the optical bias dither frequency of 0.75 Hz. Because of the difficulty in extracting data from the output autocorrelation plots, the autocorrelation function was used as an interim step to obtain the power spectral density function which was then used to design the shaping filters. The output power spectral density obtained from the autocorrelation function is shown in Figure 12. The magnitude of the first peak which occurs at 0.75 Hz, is -54 dB or $(.003 \text{ pulses}/.06 \text{ sec})^2/\text{Hz}$. The two remaining peaks occur at the third and fifth harmonic of the dither frequency. Repeatability of the test data is demonstrated by comparison of Figures 12 and 13. The two power spectral densities, computed from different data runs, are essentially identical. The spike which occurs at the origin is indicative of a random constant in the test data. Based on 12 data runs, the Gyro C turn-on to turn-on data varied between -86 dB and -94 dB.

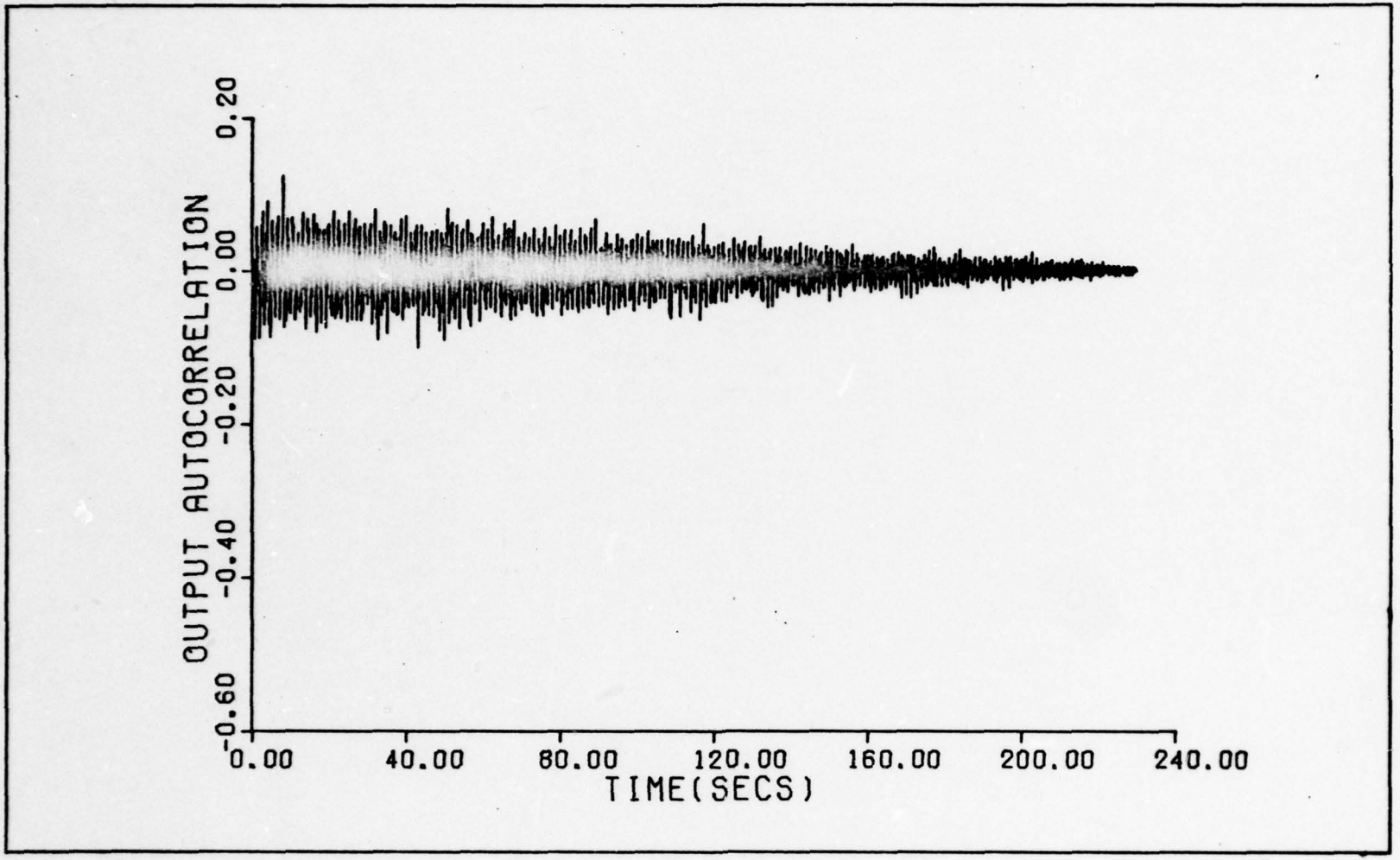

Figure 11 Gyro C Normal Operation Output Autocorrelation

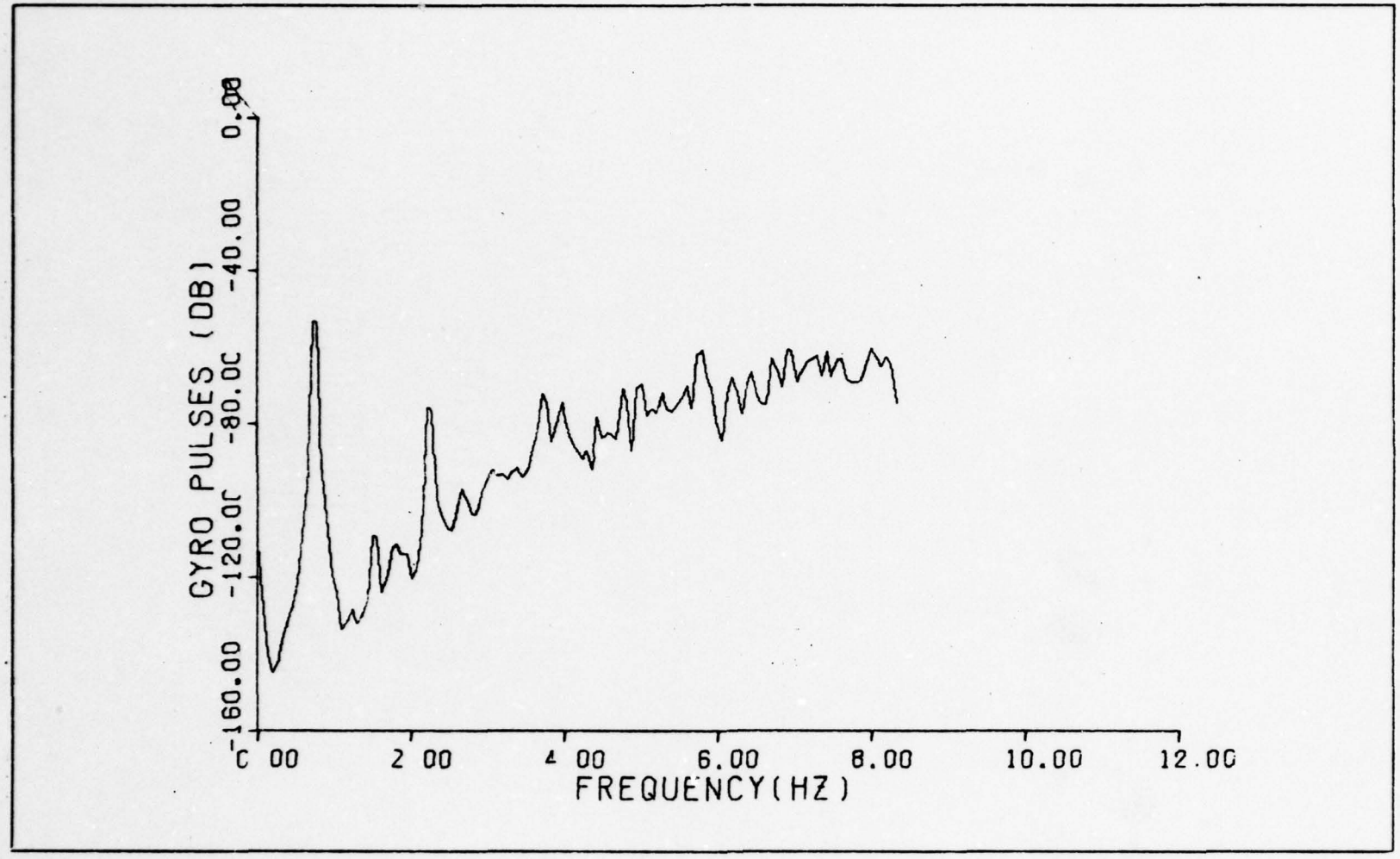

Figure 12 Cyro C Power Spectral Density--Normal Cperation

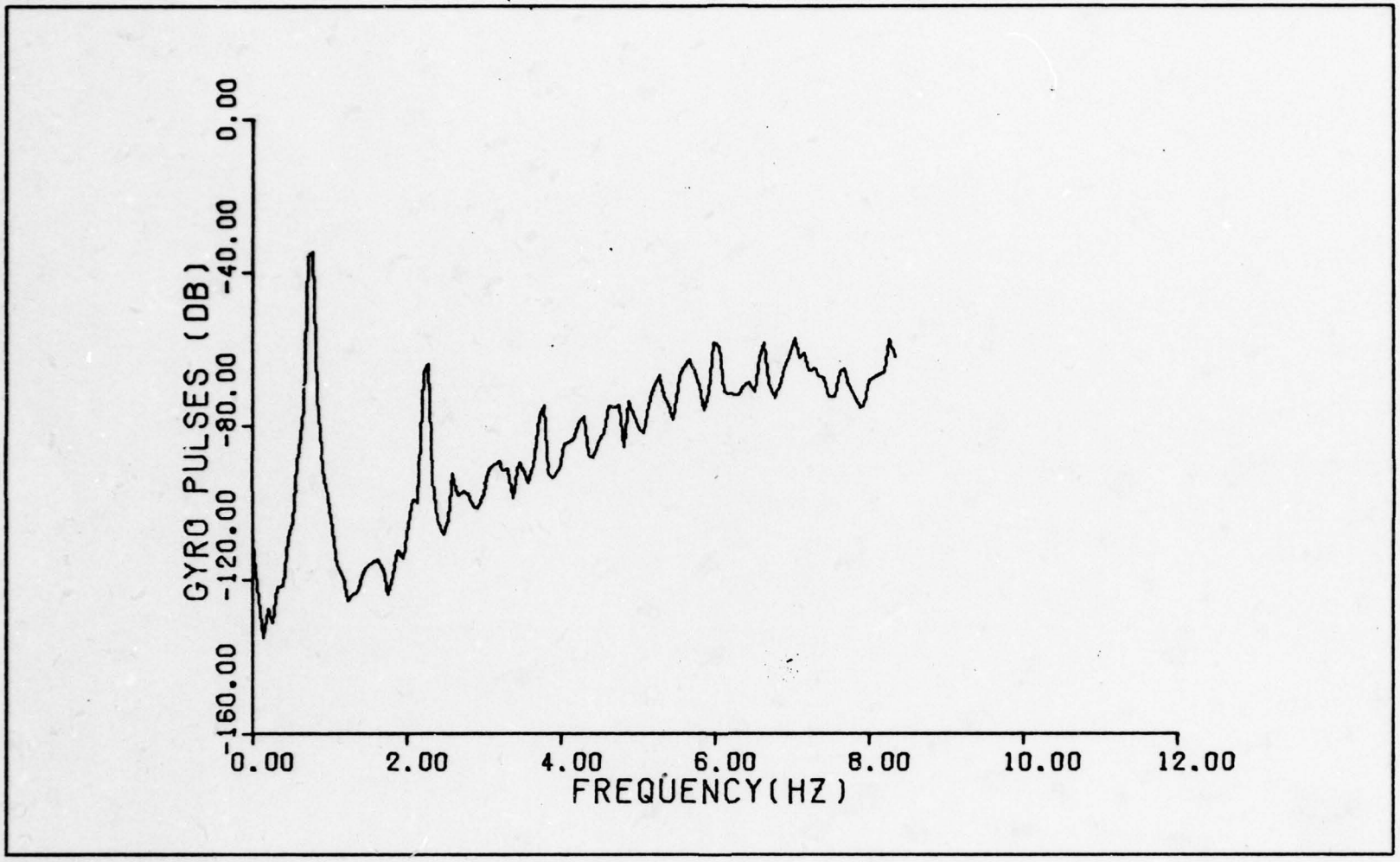

Figure 13 Gyro C Power Spectral Density--Normal Operation

The Gyro C power spectral density for operation with a constant fixed optical bias and an alternating algebraic compensation pulse train is shown in Figure 14. The peaks, which occur at the dither frequency and multiples thereof, are due to the algebraic compensation pulse train. The pulse train is subtracted from the gyro output to correct for the applied optical bias. Therefore, with the optical bias fixed and constant the output of the gyro alternated at the 0.75 Hz dither frequency. This is evident in the peaks of the power spectral density which again occur at the first, third, and fifth harmonic of the dither frequency. The spectral content of this operational mode is very nearly identical with Figures 12 and 13.

The power spectral density for operation of the gyro with an alternating optical bias and no algebraic compensation is shown in Figure 15. As in the previous operational modes, the gyro output alternates at the dither frequency. The spectral content of this operational mode is nearly identical with the previous modes except that the magnitude of the first peak is slightly greater (16 dB greater) and wider in frequency than the other modes and the third spike at 3.75 Hz is nearly lost in the background noise. However, the background noise is essentially identical between the three operational modes investigated up to this point.

Finally, the power spectral density for gyro operation with a fixed optical bias and no compensation is shown in Figure 16. Several features in this plot immediately become

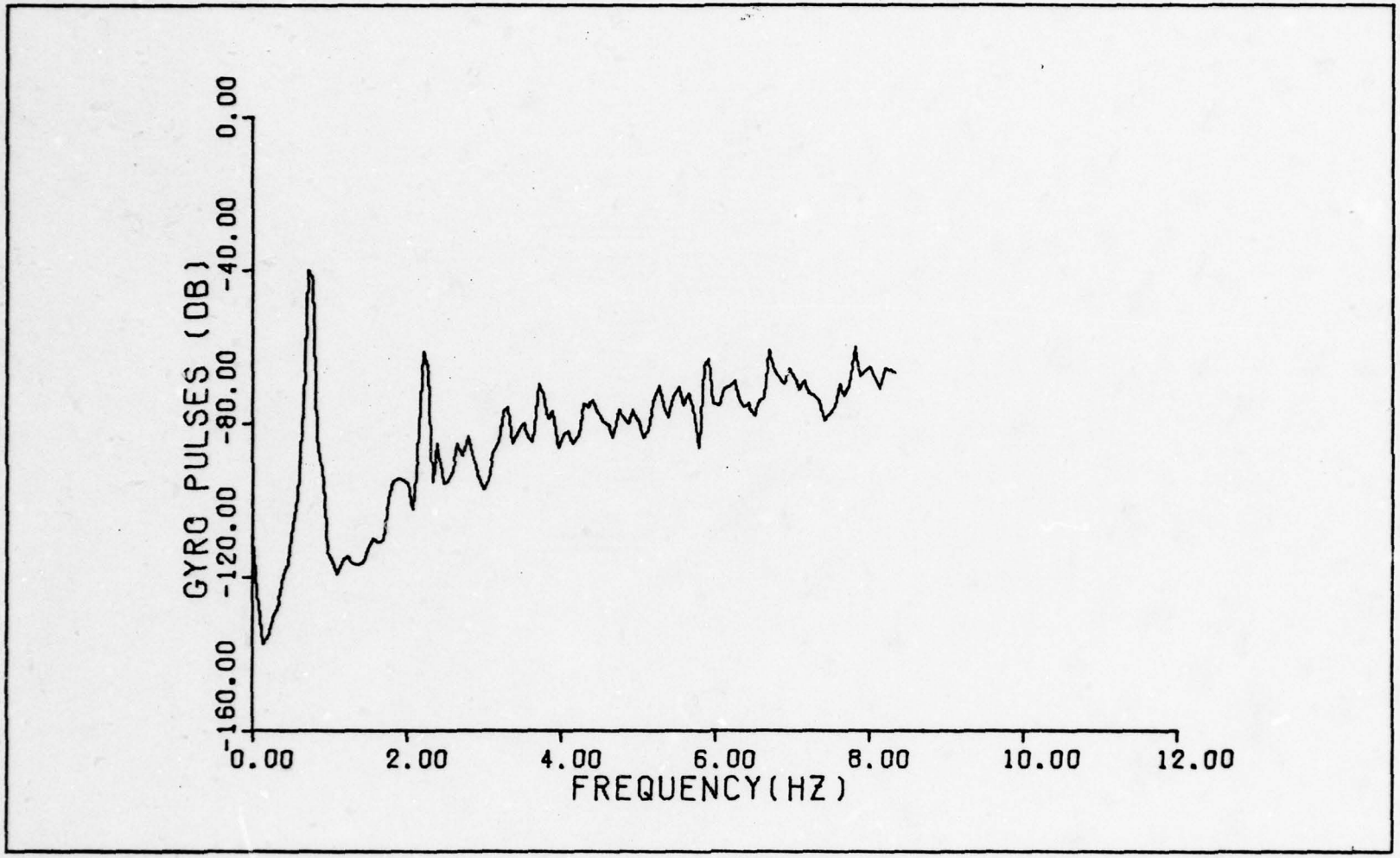

Figure 14 Gyro C Power Spectral Density--Fixed Bias, Alternating Compensation

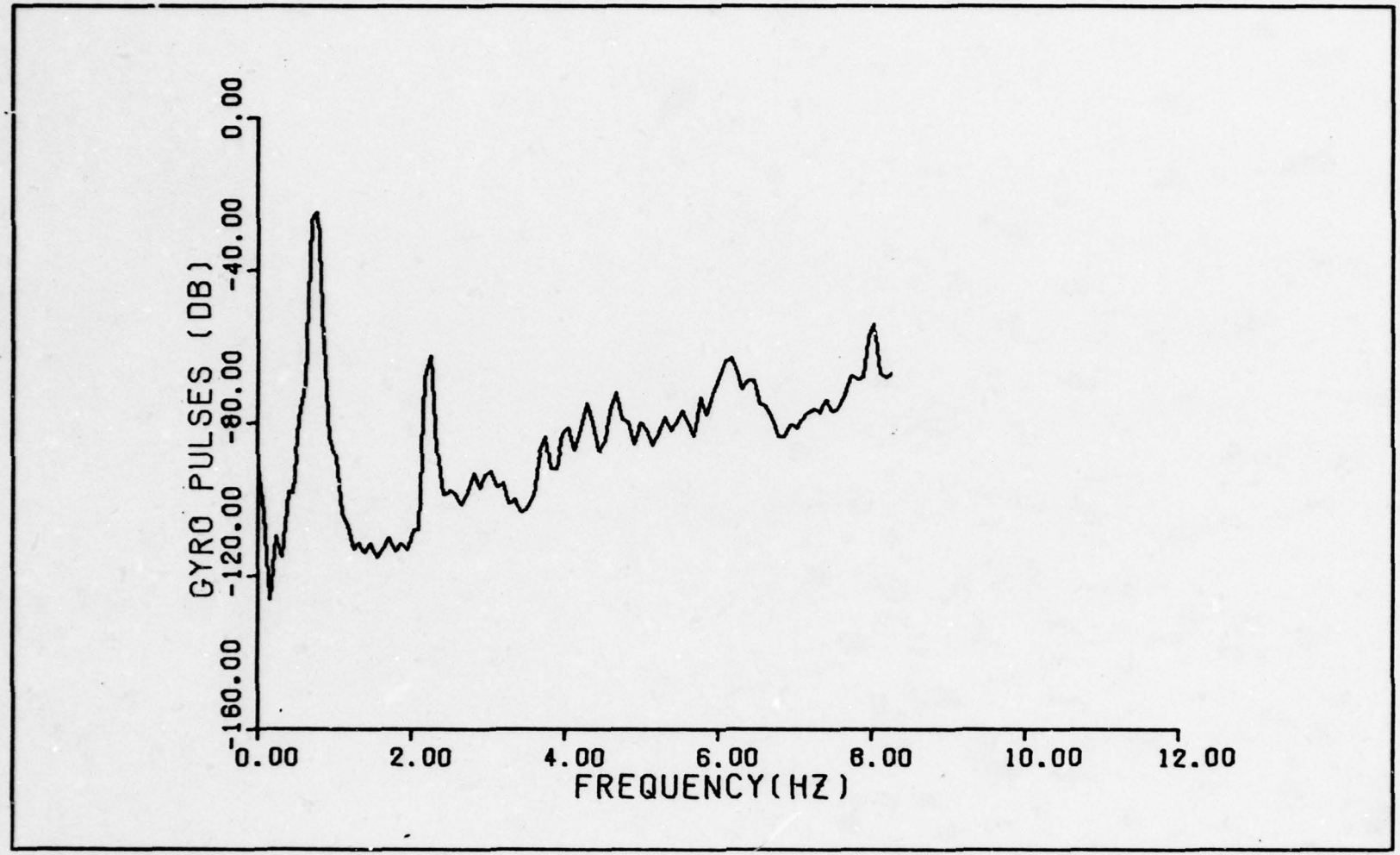

Figure 15 Gyro C Power Spectral Density--Alternating Bias, No Compensation

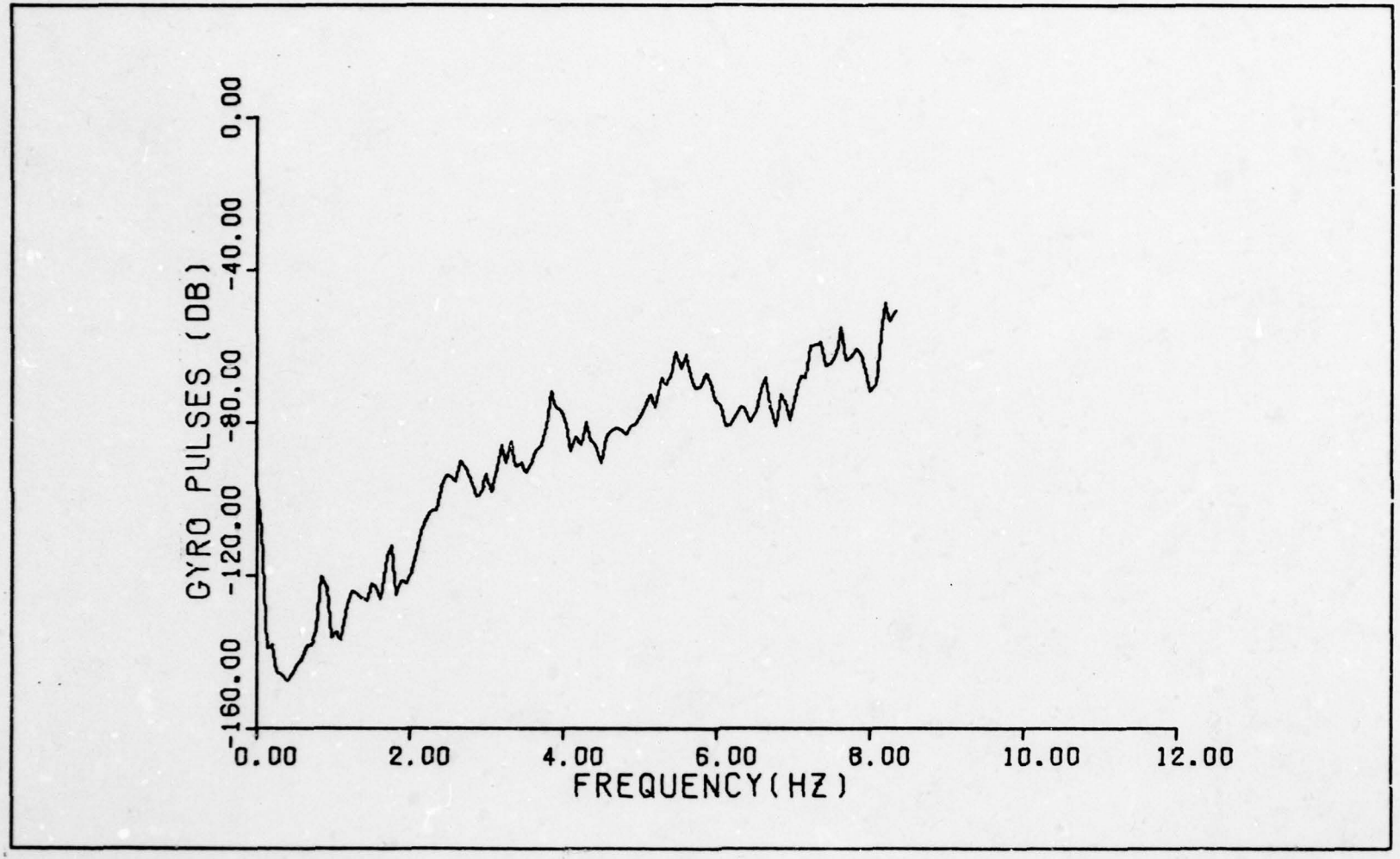

Figure 16 Gyro C Power Spectral Density--Fixed Bias, No Compensation

apparent. First, the power spikes at the first, third, and fifth harmonic of the dither frequency are gone. In addition, the background noise in this plot is the same as the background noise derived from the three previous operational modes investigated. This is graphically illustrated by comparing the power spectral density of Figure 16 with that of the background noise in Figures 12 and 13. Except for the first, third, and fifth harmonic of the dither frequency, the power spectral densities in Figures 12 and 13 closely match the power spectrum in Figure 16. Figure 17 shows the Gyro A power spectral density for fixed bias and no algebraic compensation. Although the shape of the power spectral density below 3 Hz is different from Gyro C, the peaks due to the dither frequency are also absent. Thus, even though the background noise is different between Gyros A and C, the effect of the optical dither and its compensating pulse train can be characterized by the addition of the three power spectral density spikes to the no dither noise at the first, third, and fifth harmonic of the dither frequency.

Error Models

The final step in this study was to synthesize a mathematical error model to duplicate the output noise characteristics of the SLG-15 laser gyro with and without dither. This can be accomplished by designing a shaping filter, driven by white Gaussian noise, that would reproduce the power spectral densities derived from the test data. The relationship of the output power spectral density to the input power

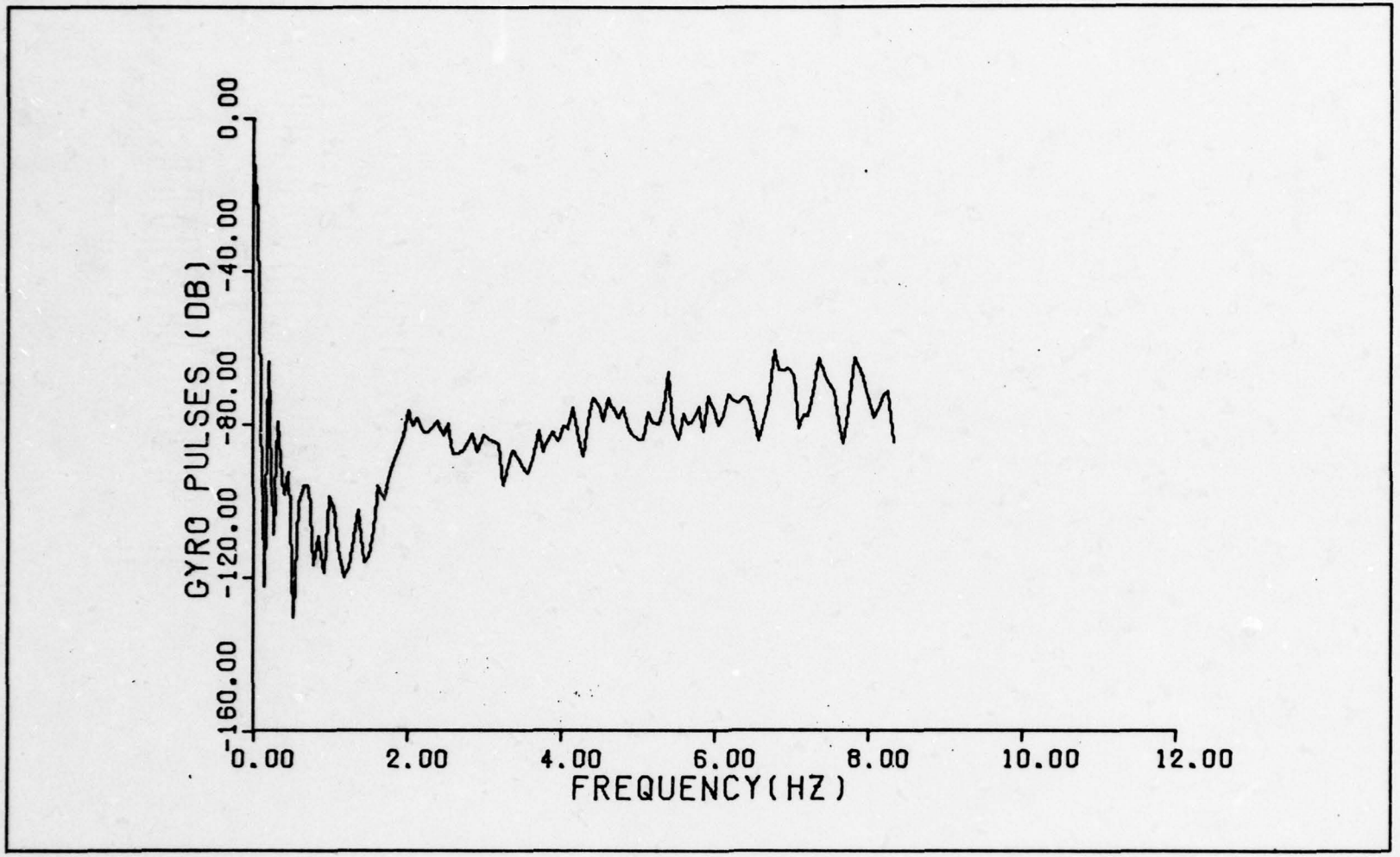

Figure 17 Gyro A Power Spectral Density--Fixed Bias, No Compensation

spectral density may be derived from the relationships relating the input and output autocorrelation functions.

A linear system may be characterized by its response to a unit impulse function. The convolution integral mathematically relates the input and output in terms of the unit impulse response

$$f_o(t) = \int_{-\infty}^{\infty} h(v) f_i(t-v)\, dv \tag{20}$$

where $f_o(t)$ is the system output, $h(v)$ is the impulse response, and $f_i(t-v)$ is the system input delayed v seconds. The transfer function relating the system output to the system input is

$$G(j\omega) = \frac{F_o(j\omega)}{F_i(j\omega)} \tag{21}$$

where $F_i(j\omega)$ and $F_o(j\omega)$ are the complex amplitudes of the input and output respectively. Therefore, the impulse response and the transfer function are Fourier transform pairs of each other and may be expressed as

$$h(t) = \frac{1}{2\pi} \int_{-\infty}^{\infty} G(j\omega)\, e^{j\omega t}\, d\omega \tag{22}$$

and

$$G(j\omega) = \int_{-\infty}^{\infty} h(t)\, e^{-j\omega t}\, dt \tag{23}$$

The output autocorrelation may be expressed as

$$\phi_{oo}(\tau) = \lim_{T\to\infty} \frac{1}{2T} \int_{-T}^{T} f_o(t) f_o(t+\tau)\, dt \tag{24}$$

Expressing the elements of the integral in terms of the convolution integral gives

$$\phi_{oo}(\tau) = \lim_{T\to\infty} \frac{1}{2T} \int_{-T}^{T} dt \int_{-\infty}^{\infty} h(v) f_i(t-v)\, dv \int_{-\infty}^{\infty} h(\delta) f_i(t+\tau-\delta)\, d\delta \tag{25}$$

Interchanging the order of integration gives

$$\phi_{oo}(\tau) = \int_{-\infty}^{\infty} h(v)\, dv \int_{-\infty}^{\infty} h(\delta)\, d\delta \lim_{T\to\infty} \frac{1}{2T} \int_{-T}^{T} f_i(t-v) f_i(t+\tau-\delta)\, dt \tag{26}$$

Now since the input autocorrelation may be expressed as

$$\phi_{ii}(\tau+v-\delta) = \lim_{T\to\infty} \frac{1}{2T} \int_{-T}^{T} f_i(t-v) f_i(t+\tau-\delta)\, dt \tag{27}$$

The output autocorrelation may be written as

$$\phi_{oo}(\tau) = \int_{-\infty}^{\infty} h(v)\, dv \int_{-\infty}^{\infty} h(\delta)\, d\delta\, \phi_{ii}(\tau+v-\delta) \tag{28}$$

The output power spectral density may be found by taking the Fourier transform of Equation (28)

$$\Phi_{oo}(\omega) = \int_{-\infty}^{\infty} e^{-j\omega\tau}\, d\tau \int_{-\infty}^{\infty} h(v)\, dv \int_{-\infty}^{\infty} h(\delta)\, d\delta\, \phi_{ii}(\tau+v-\delta) \tag{29}$$

By letting $x = \tau + v - \delta$ Equation (29) becomes

$$\Phi_{oo}(\omega) = \int_{-\infty}^{\infty} e^{-j\omega(x+\delta-v)} dx \int_{-\infty}^{\infty} h(v)dv \int_{-\infty}^{\infty} h(\delta)d\delta\, \phi_{ii}(x) \qquad (30)$$

Interchanging the order of integration and rearranging terms gives

$$\Phi_{oo}(\omega) = \int_{-\infty}^{\infty} h(v)e^{j\omega v} dv \int_{-\infty}^{\infty} h(\delta)e^{-j\omega\delta} d\delta \int_{-\infty}^{\infty} \phi_{ii}(x)e^{-j\omega x} dx \qquad (31)$$

Recalling Equations (12), and (23), the above equation may be rewritten as

$$\Phi_{oo}(\omega) = G(j\omega)\,G(-j\omega)\;\Phi_{ii}(\omega) \qquad (32)$$

Where $G(j\omega)$ and $G(-j\omega)$ are complex conjugates of each other and $G(j\omega)$ is the transfer function describing the shaping filter and $\Phi_{oo}(\omega)$ and $\Phi_{ii}(\omega)$ are the output and input power spectral densities respectively (Ref 11:4-96). Note that since the power spectral densities are always real functions, they are always even functions of $j\omega$.

The Gyro C output power spectral density, shown in Figure 16, for operation with a fixed optical bias and no algebraic compensation was fit to a curve described by

$$\Phi_{oo}(\omega) = \frac{K^2(1 + 7.73\omega^4)}{1 + .0278\omega^2} \qquad (33)$$

where $K^2 = 1.58 \times 10^{-4}$ and ω is the frequency in Hertz. A plot of Equation (33) is shown in Figure 18. The fit of the curve was accomplished by combining straight line functions whose slopes were an even multiple of 40 dB/decade on semi-log paper until a suitable fit to the data was found. The 40 dB/decade criterion was used because the resulting function is always an even multiple of $j\omega$. Thus, the fitting of the data, which is similar to a Bode plot analysis, would also produce the transfer function of the shaping filter, driven by white noise of strength equal to one, with a transfer function given by

$$G(j\omega) = \frac{K(1 + 2.36\, j\omega - 2.78\,\omega^2)}{1 + .17\, j\omega} \qquad (34)$$

It should be noted that because the numerators in both Equations (33) and (34) are of a higher order than the denominators, these functions imply an ever increasing power spectral density and hence, infinite power which is a physical impossibility. Therefore, any attempt to define a shaping filter using the transfer function in Equation (34) would be futile since the variance of the test data can only be related to the strength of the white noise driving the shaping filter in the steady state condition. However, infinite power models are used to generate error models. For example, white noise, which contains infinite power is used to drive a shaping filter which produces a finite power level over a particular frequency range or system bandpass. Thus, within the bandpass

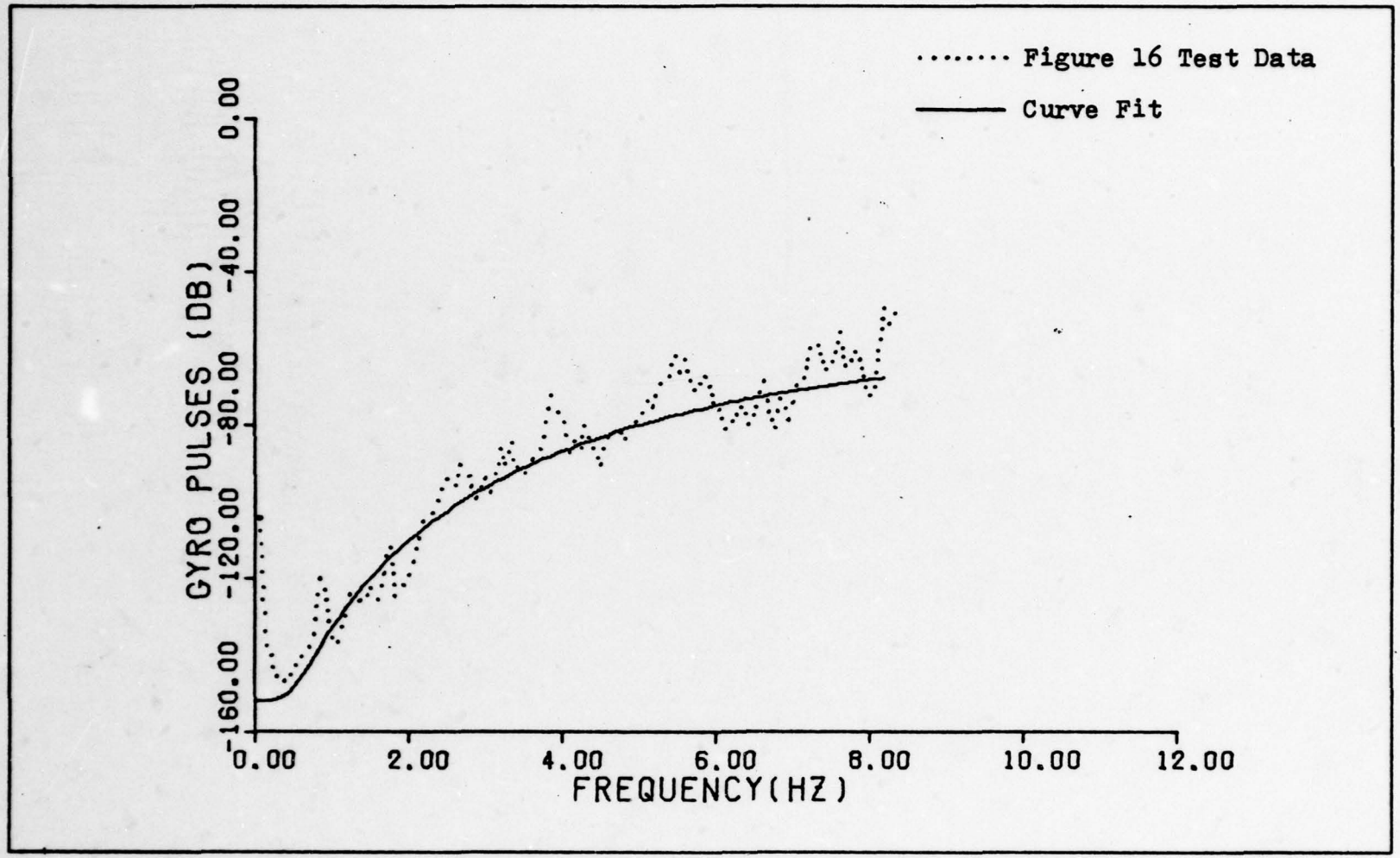

Figure 18 Gyro C Power Spectral Density Curve Fit--Fixed Bias, No Compensation

of the shaping filter, the output of the filter looks identical to the power limited noise of the system being modeled. The output of the shaping filter is then used as an input to a linear system model. Furthermore, the linear model of the physical system can be driven by white Gaussian noise in order to represent wideband noises with essentially constant power over the system bandpass. Therefore, a navigation system model could be driven by the infinite power error model in Equation (34) by limiting the system to low frequencies (below 8.33 Hz) or by attenuating the error model above 8.33 Hz. Attenuation could be accomplished by adding a second or higher order term to the denominator of the error model corresponding to the actual or desired upper cutoff frequency of the gyro.

The additional effect of dither to the power spectral density can be described by

$$\Phi_{oo}(\omega)_{TOTAL} = A_1(\omega)\, B_1(\omega)\, C_1(\omega)\, \Phi_{oo}(\omega)_{ORIGINAL} \qquad (35)$$

where A_1 is the power spectral density component at 0.75 Hz that was fit to a curve described by

$$A_1(\omega) = \frac{\left[(.5625-\omega^2)^2 + .058\omega^2\right]^2}{\left[(.5625-\omega^2)^2 + .0002\omega^2\right]^2} \qquad (36)$$

where ω is the frequency in Hertz. The fit of the curve to the data was accomplished using functions whose Bode plots were even multiples of 40 dB/decade. The magnitude and width of

the spikes were adjusted by varying the relative strength of the second order terms in the numerator and denominator. The power spectral density component at 2.25 Hz is

$$B_1(\omega) = \frac{\left[(5.063-\omega^2)^2 + .073\omega^2\right]^2}{\left[(5.063-\omega^2)^2 + .008\omega^2\right]^2} \qquad (37)$$

Similarly, the component at 3.75 Hz is

$$C_1(\omega) = \frac{\left[(14.063-\omega^2)^2 + .069\omega^2\right]^2}{\left[(14.063-\omega^2)^2 + .022\omega^2\right]^2} \qquad (38)$$

Therefore, the power density spectrum of Gyro C in the normal mode of operation can be mathematically described by cascading the effects due to dither with the description of the wideband noise from Equation (33) which gives

$$\Phi(\omega) = \frac{K^2(1+7.73\omega^4)}{1+.0278\omega^2} A_1(\omega) \cdot B_1(\omega) C_1(\omega) \qquad (39)$$

where $\Phi(\omega)$ is the output power spectral density at frequency ω, measured in Hertz, K equals 1.58×10^{-4} and functions $A_1(\omega)$, $B_1(\omega)$, and $C_1(\omega)$ are given in Equations (36), (37) and (38) respectively. A plot of Equation (39) is shown in Figure 19 for comparison with the actual test data shown in Figures 12 and 13. The math model closely agrees with the test data except that the bandwidth of the first spike is slightly narrow. This is particularly evident in comparing

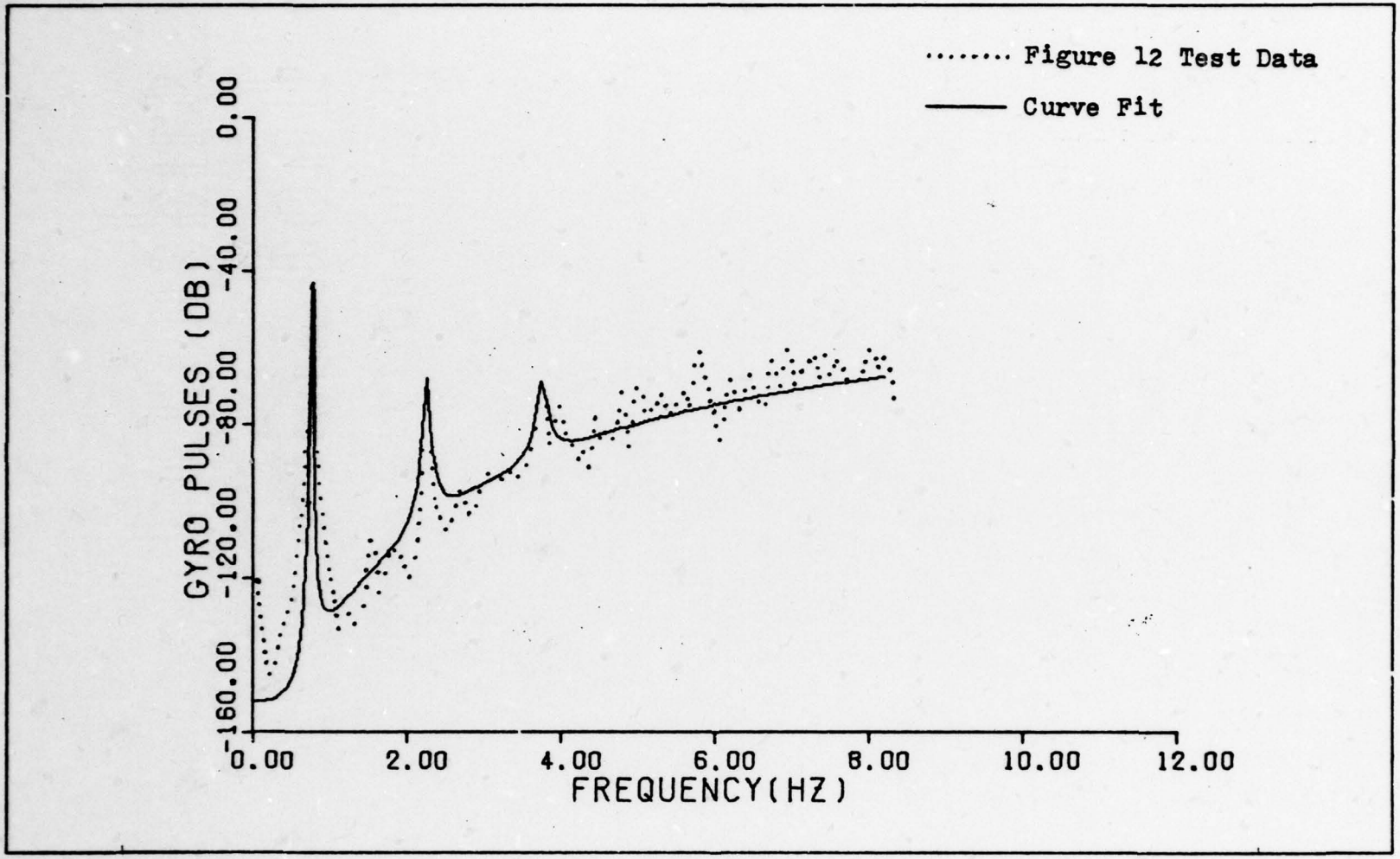

Figure 19 Gyro C Power Spectral Density Curve Fit--Normal Operation

Figure 19 with Figure 15. Figure 15 shows the power spectrum resulting from operation with an alternating bias only. The area or power contained under the first peak is larger than that contained under the first peak of the math model. Since the peak is extremely large, roughly 100 dB in magnitude, the math model for this spike is very sensitive and any changes to increase the width of the spike have a profound effect on the height of the spike. One method to minimize the sensitivity of the shape of the resonance on any one parameter of the shaping filter is to use a higher order filter. The math models were left in the format of Equations (36), (37), and (38) in order to facilitate identification of the transfer functions that would produce the power spectral density spikes when cascaded with the fixed bias, no compensation, error model given in Equation (34). The transfer functions are computed as (Ref 12:252)

$$A_1(j\omega) = \frac{\left[1 + .043\,j\omega + 1.778\,\omega^2\right]^2}{\left[1 + .027\,j\omega + 1.778\,\omega^2\right]^2} \tag{40}$$

$$B_1(j\omega) = \frac{\left[1 + .053\,j\omega + .198\,\omega^2\right]^2}{\left[1 + .018\,j\omega + .198\,\omega^2\right]^2} \tag{41}$$

$$C_1(j\omega) = \frac{\left[1 + .019\,j\omega + .071\,\omega^2\right]^2}{\left[1 + .011\,j\omega + .071\,\omega^2\right]^2} \tag{42}$$

Therefore, given an error model which describes the wide-band noise, the three notch filters whose transfer functions are given in Equations (40), (41), and (42) will adequately describe the output power spectral density of the SLG-15 laser gyro, with dither, when cascaded with the error model. The turn-on to turn-on variation was not modeled but could have been with an integrator whose only input is a random initial condition. The effect of the dither on the output may be removed by eliminating the three notch filters from the error model.

V. Conclusions and Recommendations

Conclusions

Based on analysis of the test data collected during this investigation, the system, including the algebraic compensation, used to dither the optical bias of the SLG-15 laser gyro has a profound effect on the low frequency output noise of the gyro. The test results clearly showed the existence of spikes in the output power density spectrum at the first, third, and fifth harmonic of the dither frequency. Furthermore, whenever the dither was removed from the system, the spikes were absent from the power spectral density. Although, the test data showed the wideband noise was different for Gyro A and Gyro C, comparison of Figures 12, 16, and 17 illustrated that the noise due to dither was predictable and could be added to the individual wideband noise to characterize the output of a particular gyro. Thus the low frequency noise due to dither is a characteristic of the dither mechanism and not a characteristic of the dither mechanism and not a characteristic of a particular SLG-15 gyro.

Analysis of the test data was accomplished using autocorrelation techniques to characterize the random noise output of the gyro. The technique is well suited to analysis of digital data and, with the aid of a computer, large amounts of data can be analyzed in a reasonable amount of time. Run to run comparisons of the test data showed that the data was repeatable in the 229 second test period over the 0 to 8.33 Hz range. The test results, particularly the values

of the mean and the variance, are sensitive to the test initialization, therefore test data must be collected over whole integers of the dither cycle.

The final step in the study was to synthesize an error model to duplicate the output noise of the gyro with and without dither. A math model was designed (see p.) to reproduce the effect of dither on the wideband noise spectrum of Gyro C. Therefore, given an error model which describes the fixed bias, no compensation noise spectrum, the three notch filters derived from the math model could be cascaded with the wideband model to reproduce the gyro noise.

Recommendations

The following recommendations are made for continued study and testing in the subject area of the thesis:

1. The noise of the SLG-15 laser gyro should be investigated beyond 8.33 Hz to determine the upper cutoff frequency of the gyro and a suitable shaping filter developed.

2. Another type of dither mechanism should be investigated in order to determine the effect of different mechanisms on the shape and magnitude of the power density spikes. This implies that a laser gyro with an alternate dither mechanism is available.

3. A Fourier analysis should be conducted to determine the precise shape of the time function that would produce the notch filter power spectral density spikes for normal operation of the gyro. A limited analysis showed that the relative

magnitude of the three spikes did not match the power spectral density of an ideal square wave.

4. Use of a mini-computer to buffer and pre-integrate the IMU output before placing the data onto a tape or into a Fourier analyzer would extend the present inertial navigation laboratory capability significantly.

Bibliography

1. Heller, W. G. Models for Aided Inertial Navigation System Sensor Errors. TR-312-3. Reading, Massachusetts: The Analytic Sciences Corporation, February 8, 1975.

2. Maybeck, P. S. The Kalman Filter, An Introduction for Potential Users. TM-72-3. Wright-Patterson Air Force Base, Ohio: Air Force Flight Dynamics Laboratory, 1972.

3. Operation and Service Manual, Sperry Inertial Measurement Unit (IMU), Part Number 4331-704792. Sperry Report Number 60720-1, Revision B. Great Neck, New York: Sperry Gyroscope Company, November 15, 1974, revised February 27, 1976.

4. Post, E. J. "Sagnac Effect", Reviews of Modern Physics Vol 14, No. 2: 475-493, April, 1967.

5. Aronowitz, F. "The Laser Gyro", Laser Applications, Vol 1. New York: Academic Press, Inc., 1971.

6. Steele, E. L. Optical Lasers in Electronics. New York: John Wiley and Sons, Inc., 1968.

7. Engineering Services for Recalibration of Sperry SLIC-15 Inertial Measurement Unit Serial No. 002 for Air Slew Maneuver Tests. Sperry Report Number 20229-1. Great Neck, New York: Sperry Gyroscope Division, February, 1977.

8. Modification of SLIC-15 IMU S/N 002 for Air Slew Missile Lab Experiments. unpublished Sperry Gyroscope Company paper.

9. Bias Tracker Operation. unpublished Sperry Gyroscope Company paper.

10. Bergland, G. D. "A Guided Tour of the Fast Fourier Transform", IEEE Spectrum: 41-52, July 1969

11. Maybeck, P. S. Stochastic Models, Estimation and Control. (tentative title), unpublished text. School of Engineering, Air Force Institute of Technology, Wright-Patterson AFB, Ohio, 1978.

12. D'Azzo, J. J. and C. H. Houpis. Linear Control System Analysis and Design. New York: McGraw-Hill Book Co., 1975.

Vita

Philip Alfred Renaud was born on 24 September 1944 in Northampton, Massachusetts to Phillibert F. and Theodora S. Renaud. He graduated from Amherst Regional High School, Amherst, Massachusetts in 1962 and received a Bachelor of Science degree from the University of Massachusetts in Aerospace Engineering in 1969. He was commissioned a 2/Lt, in the United States Air Force through the AFROTC program and worked as a designer with Boeing Company, Kent, Washington, on the SRAM missile program prior to entering the Air Force. He was then assigned to the Service Engineering Division, Sacramento ALC, McClellan AFB for four years where he managed airborne testing of the 120 million dollar SEAOR-62 airborne command and control radar early warning system and later worked as chief aerodynamicist on the F-105, F-104, and EC-121 aircraft. In 1973, he was selected to attend the first USAF Test Pilot School Flight Test Engineer Course at Edwards AFB. Upon graduation in 1974, he was reassigned to Sacramento ALC where he worked as the F-111D Flight Test Director. Captain Renaud entered the Air Force Institute of Technology Resident School of Engineering in pursuit of a Master's Degree in Astronautical Engineering in June 1977. Captain Renaud is married and has one daughter.

Permanent address: 10413 S. E. 174th Street
Renton, Washington

This thesis was typed by Andrea Renaud

UNCLASSIFIED
SECURITY CLASSIFICATION OF THIS PAGE (When Data Entered)

REPORT DOCUMENTATION PAGE		READ INSTRUCTIONS BEFORE COMPLETING FORM
1. REPORT NUMBER AFIT/GA/EE/78-5	2. GOVT ACCESSION NO.	3. RECIPIENT'S CATALOG NUMBER
4. TITLE (and Subtitle) GYROSCOPE ERROR MODEL INVESTIGATION FOR THE SPERRY SLIC-15 RING LASER GYROSCOPE		5. TYPE OF REPORT & PERIOD COVERED MS Thesis 6. PERFORMING ORG. REPORT NUMBER
7. AUTHOR(s) Philip A. Renaud Captain		8. CONTRACT OR GRANT NUMBER(s)
9. PERFORMING ORGANIZATION NAME AND ADDRESS Air Force Institute of Technology (AFIT/EN) Wright-Patterson AFB, Ohio 45433		10. PROGRAM ELEMENT, PROJECT, TASK AREA & WORK UNIT NUMBERS
11. CONTROLLING OFFICE NAME AND ADDRESS Air Force Avionics Laboratory/RWA-2 Wright-Patterson AFB OH 45433		12. REPORT DATE December, 1978 13. NUMBER OF PAGES
14. MONITORING AGENCY NAME & ADDRESS (if different from Controlling Office)		15. SECURITY CLASS. (of this report) Unclassified 15a. DECLASSIFICATION/DOWNGRADING SCHEDULE

16. DISTRIBUTION STATEMENT (of this Report)

Approved for public release; distribution unlimited

17. DISTRIBUTION STATEMENT (of the abstract entered in Block 20, if different from Report)

18. SUPPLEMENTARY NOTES

Approved for public release: IAW AFR 190-17

J. P. Hipps, Major, USAF
Director of Information 1-23-79

19. KEY WORDS (Continue on reverse side if necessary and identify by block number)

Laser Gyro
Gyro noise
Error model

20. ABSTRACT (Continue on reverse side if necessary and identify by block number)

Power spectral density measurements from 10-3 to 8.33 Hz are made of the output noise of the SLG-15 laser gyroscope used in the SLIC-15 IMU manufactured by Sperry Gyroscope Company. A detailed discussion of the operation of the SLG-15 laser gyro is presented along with a description of its optical dither mechanism. The digital output of the gyroscope is analyzed using correlation techniques to characterize the noise. A description of the analysis technique and the test station used for the measurements is>

DD FORM 1 JAN 73 1473 EDITION OF 1 NOV 65 IS OBSOLETE

UNCLASSIFIED
SECURITY CLASSIFICATION OF THIS PAGE (When Data Entered)

20. given along with representative samples of the output noise. Particular attention is paid to the effect of the dither mechanism on the output power density spectrum. The tests show that the low frequency noise due to dither is a characteristic of the dither mechanism and not a characteristic of a particular SLG-15 laser gyro. Based on the test data a linear low frequency model is constructed for both the dithered and undithered case.